

Fra-2-expressing macrophages promote lung fibrosis

Alvaro C. Uceró,¹ Latifa Bakiri,¹ Ben Roediger,^{1,2,3} Masakatsu Suzuki,⁴ Maria Jimenez,¹ Pratyusha Mandal,⁵ Paola Braghetta,⁶ Paolo Bonaldo,⁶ Luis Paz-Ares,⁷ Coral Fustero-Torre,⁸ Pilar Ximenez-Embun,⁹ Ana Isabel Hernandez,¹⁰ Diego Megias,¹¹ and Erwin F. Wagner¹²

¹Genes, Development and Disease Group, Cancer Cell Biology Programme, Spanish National Cancer Research Centre (CNIO), Madrid, Spain. ²Skin Imaging and Inflammation Laboratory, The Centenary Institute, Newtown, Australia. ³Sydney Medical School, University of Sydney, Camperdown, New South Wales, Australia. ⁴End-Organ Disease Laboratories, R&D Division, Daiichi Sankyo Company, Tokyo, Japan. ⁵Department of Microbiology and Immunology, Emory Vaccine Center, Emory University School of Medicine, Atlanta, Georgia, USA. ⁶Department of Molecular Medicine, University of Padova, Padova, Italy. ⁷Lung Cancer Clinical Research Unit H120-CNIO. ⁸Bioinformatics Unit, Structural Biology and Biocomputing Programme, ⁹ProteoRed-ISCI, Proteomics Unit, ¹⁰Medicinal Chemistry Unit, Experimental Therapeutics Programme, and ¹¹Confocal Microscopy Core Unit, CNIO, Madrid, Spain. ¹²Laboratory Genes and Disease, Department of Dermatology and Department of Laboratory Medicine, Medical University of Vienna, Vienna, Austria.

Idiopathic pulmonary fibrosis (IPF) is a deadly disease with limited therapies. Tissue fibrosis is associated with type 2 immune response, although the causal contribution of immune cells is not defined. The AP-1 transcription factor Fra-2 is upregulated in IPF lung sections, and Fra-2 transgenic mice (Fra-2^{Tg}) exhibit spontaneous lung fibrosis. Here, we show that bleomycin-induced lung fibrosis is attenuated upon myeloid inactivation of Fra-2 and aggravated in Fra-2^{Tg} bone marrow chimeras. Type VI collagen (ColVI), a Fra-2 transcriptional target, is upregulated in 3 lung fibrosis models, and macrophages promote myofibroblast activation in vitro in a ColVI- and Fra-2-dependent manner. Fra-2 or ColVI inactivation does not affect macrophage recruitment and alternative activation, suggesting that Fra-2/ColVI specifically controls the paracrine profibrotic activity of macrophages. Importantly, ColVI-KO mice and ColVI-KO bone marrow chimeras are protected from bleomycin-induced lung fibrosis. Therapeutic administration of a Fra-2/AP-1 inhibitor reduces ColVI expression and ameliorates fibrosis in Fra-2^{Tg} mice and in the bleomycin model. Finally, Fra-2 and ColVI positively correlate in IPF patient samples and colocalize in lung macrophages. Therefore, the Fra-2/ColVI profibrotic axis is a promising biomarker and therapeutic target for lung fibrosis and possibly other fibrotic diseases.

Introduction

Fibrosis is the result of an abnormal healing process that can occur in every solid organ where hyperactive fibroblasts, called myofibroblasts, characterized by the expression of α -SMA, produce an excess of extracellular matrix (ECM). This accumulation of ECM ultimately alters organ structure and function (1, 2), and no treatment can halt or reverse fibrosis progression. Organ fibrosis is a leading cause of death worldwide and an important focus of research over the past years (3, 4). One dramatic example is idiopathic pulmonary fibrosis (IPF), a common manifestation of interstitial lung diseases (ILDs). IPF progression is very fast, with a median postdiagnosis survival of 2.5 years and a 20% to 30% 5-year survival rate (5). The current treatment options for IPF, including lung transplantation and the recently approved nintedanib and pirfenidone (6, 7), are limited, and there is an urgent need for new therapeutic targets.

While the participation of fibroblasts in disease progression is well accepted, whether inflammation contributes to IPF is debated. The inflammatory cell infiltrate is small compared with that of other inflammatory lung diseases, and antiinflammatory drugs

are ineffective (8–10). A common feature of wound healing and fibrosis is the long-lasting presence of alternatively activated macrophages (AAMs), which participate in the resolution of inflammation and in the fibroblast-myofibroblast conversion (4, 11–14). Macrophages also contribute to ECM remodeling by producing matrix-related proteins, such as matrix-degrading enzymes and fibronectin (15–17). AAMs have an important role in chronic diseases as well as cancer and are therapeutically relevant in preclinical models (18, 19). IL-4 and IL-13 are the main inducers of alternative macrophage activation (20). These cytokines can lead to fibrosis by direct and indirect effects on fibroblasts together with or independently of the canonical profibrotic TGF- β 1 (21, 22).

AP-1 proteins form dimers to activate or repress gene transcription in a context-dependent manner and are involved in causation of a variety of chronic diseases, from psoriasis to cancer, acting by regulating cellular processes, such as proliferation, differentiation, and inflammation (23, 24). Genetically engineered mice expressing the AP-1 transcription factor Fra-2, encoded by *Fosl2*, develop spontaneous systemic fibrosis (25). The accumulation of ECM is particularly prominent in the lungs of Fra-2 transgenic (Fra-2^{Tg}) mice and causes premature death. Furthermore, fibrotic Fra-2^{Tg} lungs display high IL-4 expression with eosinophilic and macrophage infiltration and vascular remodelling (25).

Using several preclinical models for lung fibrosis, we sought to define the cellular and molecular determinants of lung fibrosis

Conflict of interest: The authors have declared that no conflict of interest exists.

Copyright: © 2019, American Society for Clinical Investigation.

Submitted: October 5, 2018; **Accepted:** May 21, 2019; **Published:** July 15, 2019.

Reference information: *J Clin Invest.* 2019;129(8):3293–3309.

<https://doi.org/10.1172/JCI125366>.

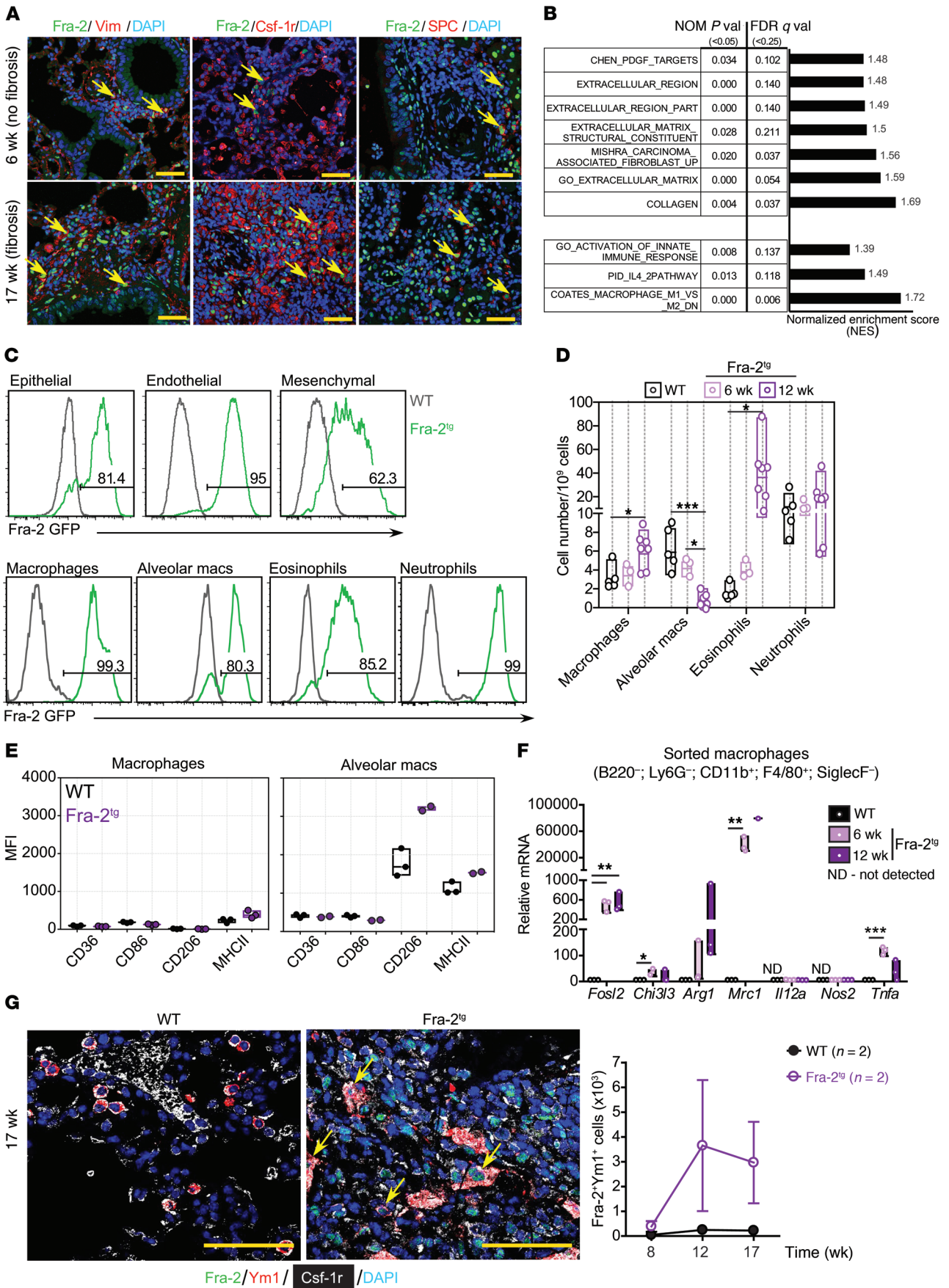


Figure 1. Alternative activation of macrophages in Fra-2^{Tg} fibrotic lungs. (A) Confocal microscopy images of IF for Fra-2 (green) and Vimentin (Vim), Csf-1r, or SPC (red). Arrows point to double-positive cells. Nuclei are counterstained with DAPI (blue). Scale bars: 25 μ m. (B) GSEA on ECM- and type 2 immunity-related pathways in Fra-2^{Tg} lungs compared with WT littermates (6 weeks, RNA-Seq, $n = 3/3$ from 1 experiment). Normalized enrichment score (NES), nominal (NOM) P values, FDR, and Q values are indicated. (C) Flow cytometry analysis on GFP expression in epithelial (CD45⁺EpCAM⁺), endothelial (CD45⁺EpCAM⁺CD31⁺), and mesenchymal (CD45⁺EpCAM⁺CD31⁺CD140a⁺) cells and in myeloid cell subpopulations in WT (black) and Fra-2^{Tg} (green) mouse lungs at 12 weeks of age. Percentages of GFP-positive cells in the plots are shown. (D) Relative myeloid subpopulation cell numbers. Experiment was repeated twice. Mean, maximum, and minimum are plotted with individual values. * $P < 0.05$; *** $P < 0.001$, 1-way ANOVA; Bonferroni's post test. Group comparisons in each cell type are shown. macs, macrophages. (E) Expression of surface markers on nonalveolar (Siglec-F⁺CD11b^{hi}F4/80⁺; left) and alveolar (Siglec-F⁺CD11b^{lo}; right) macrophages in the lungs of 12-week-old WT (black) and Fra-2^{Tg} (purple) mice. Median fluorescence intensity (MFI) is plotted. (F) qRT-PCR analysis of lung macrophages isolated by FACS ($n = 3$; biological replicates from 1 experiment). Relative expression in WT is set to 1. * $P < 0.05$; ** $P < 0.01$; *** $P < 0.001$, unpaired 2-tailed t test. (G) Left, confocal microscopy images of Fra-2 (green), Csf-1r (white), and Ym1 (red) costaining. Nuclei are counterstained with DAPI (blue). Arrows point to triple-positive cells. Scale bars: 50 μ m. Right, computational quantification of double Fra-2- and Ym1-positive cell numbers ($n = 2$; biological replicates from 1 experiment).

and evaluate the therapeutic relevance of targeting AP-1 or any of these determinants. We show that Fra-2-expressing macrophages are important contributors to lung fibrosis, secreting fibroblast-activating factors, such as type VI collagen (ColVI). Importantly, while macrophage alternative activation and Th2 immunity are overall not affected, reduced bleomycin-induced lung fibrosis is observed in mice with broad or myeloid-specific Fra-2/AP-1 inactivation as well as in ColVI KO mice and ColVI BM chimeras.

Results

AAMs are prominent in lungs of Fra-2^{Tg} mice. Immunohistological analysis of prefibrotic (before structural changes; at 6 weeks old) and fibrotic (17 weeks) Fra-2^{Tg} lungs revealed that Fra-2 protein was detectable in mesenchymal cells expressing vimentin, in cells of the monocyte/macrophage lineage expressing colony-stimulating factor 1 receptor (Csf-1r), and in surfactant-associated protein C-positive (SPC-positive) alveolar epithelial type II (AEC2) cells (Figure 1A), a cell type implicated in fibrosis and lung tissue repair (26, 27). Consistent with the early occurrence of fibrosis-associated molecular changes, mRNA expression of ECM proteins, such as type I and III collagens (*Col1a2* and *Col3a1*), or fibroblast-related genes, such as fibroblast-specific protein-1 (*S100a4*), was increased in prefibrotic (6 weeks) Fra-2^{Tg} lungs (Supplemental Figure 1, A and B; supplemental material available online with this article; <https://doi.org/10.1172/JCI125366DS1>). In Fra-2^{Tg} lung protein extracts, periostin, α -SMA, and osteopontin were increased at as early as 5, 9, and 12 weeks of age, respectively (Supplemental Figure 1C). Global gene expression analyses (RNA-Seq) and gene set enrichment analysis (GSEA) revealed positive correlation between prefibrotic Fra-2^{Tg} lungs and published gene signatures related to ECM and collagen, but also with IL-4 response and alternative activation of macrophages (Figure 1B). TGF- β pathway activation was not apparent from RNA-Seq/GSEA (not shown) or immunoblot analyses (Supplemental Figure 1D), consistent with published studies (28). GSEA also confirmed Fra-1/2 pathway activation in Fra-2^{Tg} lungs (Supplemental Figure 1E), and deconvolution into cell-specific subprofiles revealed enrichment in myeloid signatures, such as neutrophils, eosinophils, dendritic cells, and macrophages (Supplemental Figure 1F). Importantly, a significant increase in genes characteristic of AAMs, such as *Ccl17*, *Ccl22*, *Chi3l3*, *Chi3l4*, *Mrc1*, and *Arg1*, encoding for the chemokines Ccl17 and Ccl22, the chitinases Ym1 and Ym2, the mannose receptor 1/CD206, and arginase 1, respectively, was apparent in Fra-2^{Tg} lungs (Supplemental Figure 1, G and H). In contrast, markers of classically activated macrophages

(CAM), such as *Cd86*, *Irf5*, *Il1b*, and *Il12a*, were overall not consistently changed (Supplemental Figure 1, G and H). Macrophage activation is defined in vivo and in vitro by the organ source, the activator molecule, and the expression of a consensus collection of markers (29). According to this definition, gene expression profiling suggests that M(IL-4) macrophages are enriched in the lungs of young prefibrotic Fra-2^{Tg} mice.

Fra-2-expressing myeloid cell populations were next analyzed by flow cytometry using the GFP reporter included in the Fra-2 transgene and by cell-surface marker expression (Supplemental Figure 1, I and J). In prefibrotic and fibrotic Fra-2^{Tg} lungs, Fra-2 transgene expression was detected in all myeloid cell populations in proportions ranging from 70% to 90% and also in epithelial, endothelial, and mesenchymal cells (Figure 1C). A dramatic loss of resident alveolar macrophages was observed in Fra-2^{Tg} mouse lungs at 12 weeks, while macrophages and eosinophils significantly increased (Figure 1D).

Flow cytometry analyses of macrophages revealed an upregulation of AAM marker CD206 (encoded by *Mrc1*) on Siglec-F⁺CD11b^{lo} alveolar macrophages in the lungs of 12-week-old Fra-2^{Tg} mice. Although surface CD206 remained low on conventional, non-alveolar (Siglec-F⁺CD11b^{hi}F4/80⁺) macrophages (Figure 1E), gene expression analyses of a panel of CAM and AAM markers in sorted lung macrophages revealed strong upregulation of *Mrc1* transcription together with other AAM-associated genes (Figure 1F), consistent with alternative activation. Furthermore, the AAM marker Ym1 was coexpressed with Fra-2 in Csf-1r-positive macrophages in Fra-2^{Tg} lung sections, and a progressive increase in Ym1-positive and Fra-2/Ym1 double-positive cells was observed over time (Figure 1G and Supplemental Figure 1K). Overall, these data indicate that AAMs, likely with a M(IL-4) phenotype, could be a relevant early contributor to lung fibrosis in the Fra-2^{Tg} mouse model.

Fra-2 is upregulated during bleomycin-induced experimental fibrosis in mice. Intratracheal administration of the antineoplastic drug bleomycin is a well-established ILD paradigm, with fibrotic lesions developing from 1 week and progressing during 21 days, followed by slow repair or progression to death (30). The lung function decline due to tissue stiffening can be followed by longitudinal plethysmography in bleomycin-treated mice, as lung resistance (LR) increases over time, while dynamic compliance (DC) decreases, resulting in a higher LR/DC ratio (Supplemental Figure 2A).

In WT mice, Fra-2 protein was detected in lung sections as early as 10 days after bleomycin instillation (Figure 2A and Supplemental Figure 2B). mRNA expression in the lung and the bron-

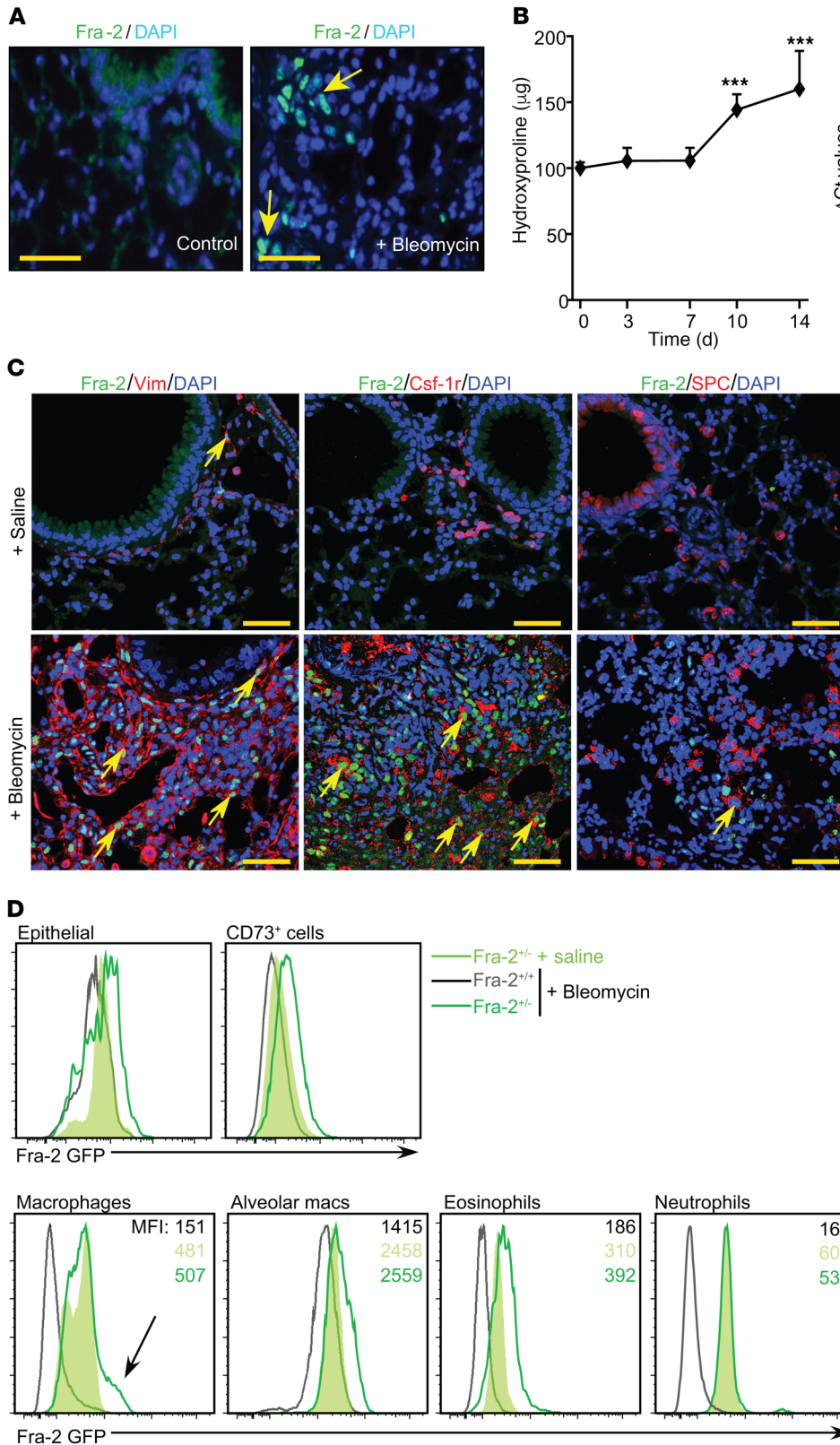


Figure 2. Fra-2 expression in bleomycin-induced lung fibrosis. (A) Fluorescence microscopy images of Fra-2 IF of lungs from WT mice 10 days after saline or bleomycin treatment. Nuclei are counterstained with DAPI. Arrows point to positive nuclei. Scale bars: 25 µm. (B) Time-course analysis of hydroxyproline accumulation and Fra-2 mRNA expression (qRT-PCR as *Fosl2*) in lungs and BALF from bleomycin-treated WT mice. ΔCt values are plotted. Sample size is *n* = 5 for lung tissue and *n* = 3 for BALF. ***P* < 0.01; ****P* < 0.001, compared with the initial time point (0 days); 1-way ANOVA; Dunnett's post test. (C) Confocal microscopy images on IF of fibrotic lungs from untreated and bleomycin-treated WT mice (14 days). Costaining for Fra-2 (green) and vimentin, Csf-1r, or SPC (red). Arrows point to double-positive cells. Nuclei are counterstained with DAPI (blue). Scale bars: 25 µm. (D) Flow cytometry analysis of lung GFP-expressing cells after 10 days of either saline or bleomycin (*n* = 3/group, from 2 independent experiments). MFI average values are presented in each plot. Arrow indicates a subpopulation of Fra-2-expressing macrophages present in bleomycin-treated mice that were absent from saline-treated controls.

chioalveolar lavage fluid (BALF) was evaluated over time (Supplemental Figure 2C). Fra-2 mRNA expression peaked in BALF and lung at 3 and 10 days after bleomycin, respectively, and preceded collagen accumulation (Figure 2B). TGF-β1 and AAM marker gene

expression increase was also detected in BALF cells and lung tissue (Supplemental Figure 2D). BALF contained high numbers of macrophages after bleomycin, while neutrophils and lymphocytes were barely detected (Supplemental Figure 2E). Fra-2 protein was

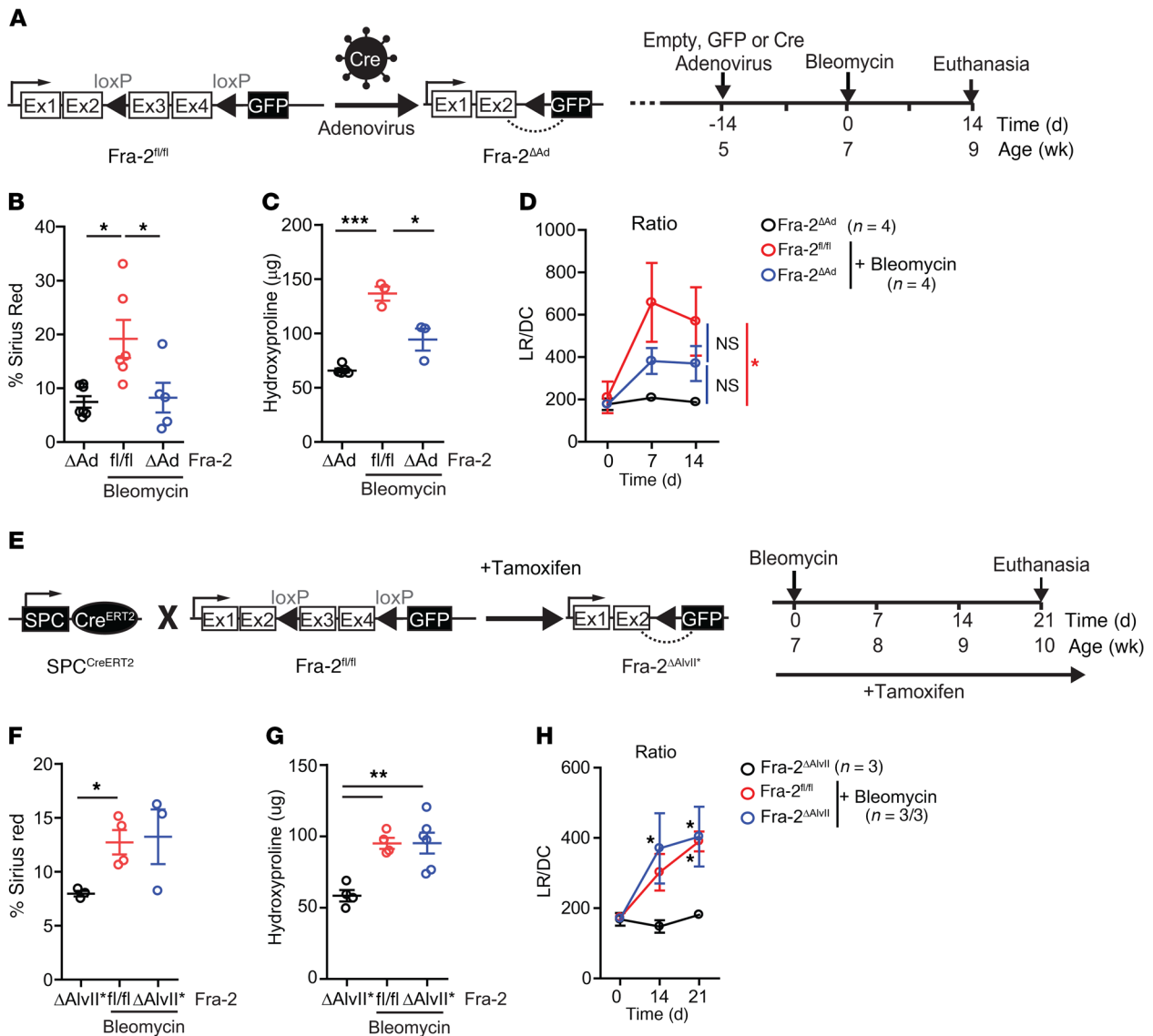


Figure 3. Fra-2 expression is essential for bleomycin-induced lung fibrosis. (A) Schematic for genetic Cre/LoxP inactivation of Fra-2 (encoded by *fosl2*) using intratracheal adenovirus-based Cre delivery (Fra-2^{ΔAd}) and experimental time line. Data come from 2 independent experiments. (B) Quantification of sirius red-positive areas 14 days after bleomycin treatment. Saline-treated Fra-2^{ΔAd} mice were used as controls. **P* < 0.05, 1-way ANOVA; Bonferroni's post test. (C) Hydroxyproline content in lungs (left lobe) 14 days after bleomycin treatment. Saline-treated Fra-2^{ΔAd} mice were used as controls. **P* < 0.05; ****P* < 0.001, 1-way ANOVA; Bonferroni's post test. (D) LR (mmHg/mL × s⁻¹) and DC (mL/mmHg) were measured by plethysmography in the same animals over time, and mean ± SEM of the LR/DC ratios were plotted. **P* < 0.05, 2-way ANOVA; Bonferroni's post test. Statistics relative to animals receiving saline. (E) Schematic for genetic Cre/LoxP inactivation of Fra-2 (encoded by *Fosl2*) using the tamoxifen-inducible, lung alveolar type II cell-specific SPC^{CreERT2} knockin allele (Fra-2^{ΔAlvII*}) and experimental time line. Experiment was repeated 3 times. (F) Quantification of lung sirius red-positive areas 21 days after bleomycin. **P* < 0.05, unpaired 2-tailed *t* test. Fibrosis was assessed in 2 independent experiments. (G) Lung hydroxyproline content 21 days after bleomycin treatment. ***P* < 0.01, 1-way ANOVA; Bonferroni's post test. Fibrosis was assessed in 2 independent experiments. (H) Respiratory function of bleomycin-treated Fra-2^{fl/fl} and Fra-2^{ΔAlvII*} mice and saline-treated Fra-2^{ΔAlvII*} mice. **P* < 0.05, 2-way ANOVA; Bonferroni's post test. Statistics are relative to mice receiving saline.

detected in mesenchymal cells and macrophages by immunofluorescence (IF) in lung sections, a pattern reminiscent of that in Fra-2^{fl/fl} lungs (Figure 1A), but not in AEC2 cells 14 days after bleomycin (Figure 2C). Fra-2^{+/-} heterozygous mice (31) expressing a GFP reporter controlled by the endogenous Fra-2 regulatory elements were monitored by flow cytometry (Supplemental Figure 3, A and B). Under homeostatic conditions, the Fra-2 GFP reporter was barely detectable in lung epithelial and CD73⁺ cells (including

fibroblast and endothelial cells), while it was expressed in alveolar and conventional macrophages, as well as in neutrophils and in eosinophils (Figure 2D). Ten days after bleomycin, Fra-2 GFP expression increased in epithelial cells, CD73⁺ cells, alveolar macrophages, eosinophils, and a subset of conventional macrophages, but not in neutrophils (Figure 2D). These results indicate that Fra-2-expressing macrophages might contribute to bleomycin-induced lung fibrosis.

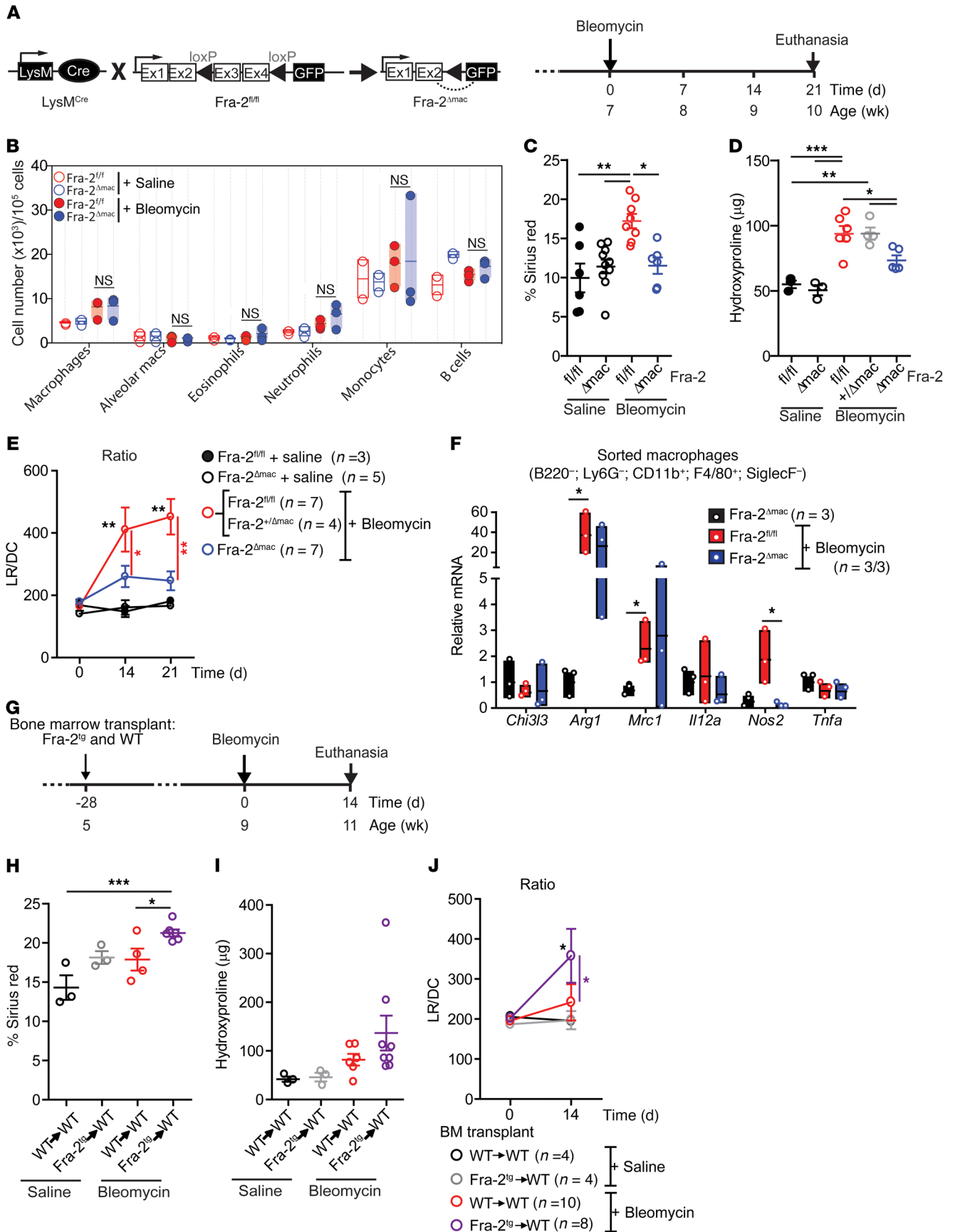


Figure 4. Bleomycin-induced lung fibrosis requires Fra-2 expression in macrophages. (A) Schematic for genetic Cre/LoxP inactivation of Fra-2 (encoded by *Fos12*) using the myeloid cell-specific *Lyz2-Cre* knockin allele (Fra-2^{Δmac}) and experimental time line. Experiment was repeated 6 times. (B) Relative myeloid subpopulation cell and B cell numbers in Fra-2^{fl/fl} and Fra-2^{Δmac} mice 10 days after saline or bleomycin treatment. (C) Quantification of sirius red-positive lung after either saline or bleomycin for 21 days. **P* < 0.05; ***P* < 0.01, 1-way ANOVA; Bonferroni's post test. (D) Lung hydroxyproline content 21 days after bleomycin treatment. **P* < 0.05; ***P* < 0.01; ****P* < 0.001, 1-way ANOVA; Bonferroni's post test. (E) Respiratory function of saline-treated Fra-2^{fl/fl} and Fra-2^{Δmac} mice and bleomycin-treated Fra-2^{fl/fl} (including Fra-2^{+/Δmac}) and Fra-2^{Δmac} mice. **P* < 0.05; ***P* < 0.01, 2-way ANOVA; Bonferroni's post test. (F) qRT-PCR analysis in isolated lung macrophages (as B220⁻, Ly6G⁻, CD11b⁺, F4/80⁺, Siglec-F⁻ cells) 10 days after bleomycin treatment (*n* = 3/group; 1 experiment). Average gene expression in saline-treated Fra-2^{Δmac} sorted cells is set to 1. **P* < 0.05, unpaired 2-tailed *t* test. (G) Schematic for experimental design and time line of saline- and bleomycin-treated WT mice transplanted with either WT BM (WT→WT) or Fra-2^{fl/fl} BM (Fra-2^{fl/fl}→WT). Bleomycin was injected into 2 independent sets of transplanted mice. (H) Quantification of sirius red-positive area in lung sections 14 days after bleomycin. Data from 2 independent experiments are plotted. **P* < 0.05, ****P* < 0.001, unpaired 1-tailed *t* test. (I) Lung hydroxyproline content 14 days after bleomycin treatment. (J) Respiratory function at 0 and 14 days after bleomycin treatment. **P* < 0.05 compared with either saline control or WT→WT bleomycin-treated group. Two-way ANOVA; Bonferroni's post test.

Fra-2 is essential for lung fibrosis development. As germline inactivation of Fra-2 is lethal (31), Fra-2 was locally inactivated in the lung of mice homozygous for a Fra-2-floxed allele (Fra-2^{fl/fl}) by intratracheal delivery of adenovirus expressing Cre recombinase (Fra-2^{ΔAd}). This method is widely used to target lung epithelial cells (32), and the resulting Fra-2^{ΔAd} mice were healthy with no lung phenotype for the duration of the experiment (Figure 3A). Flow cytometry analyses of mice treated with adenovirus expressing GFP and bleomycin revealed efficient targeting of epithelial cells, but also mesenchymal cells and all myeloid cells (Supplemental Figure 3C). Fra-2 inactivation resulted in less severe bleomycin-induced fibrosis, with decreased sirius red positivity (Figure 3B) and lower hydroxyproline content (Figure 3C) in the lungs of Fra-2^{ΔAd} mice compared with Fra-2^{fl/fl} littermates receiving empty adenovirus. Finally, longitudinal plethysmography revealed a somehow milder decline in lung function in Fra-2^{ΔAd} mice 7 and 14 days after bleomycin, with a lower LR/DC ratio compared with that of empty virus littermates (Figure 3D).

Next, Fra-2 was genetically inactivated in AEC2 lung epithelial cells by combining Fra-2 floxed alleles with the tamoxifen-inducible SPC-Cre^{ERT2} knockin allele (33). The resulting Fra-2^{ΔAlvII} mice were healthy on a tamoxifen diet with no obvious lung alterations. The GFP reporter included in the Fra-2 floxed allele and expressed instead of Fra-2 upon Cre-mediated gene deletion (Figure 3E) was only detected in a small number of epithelial cells (CD45⁺EpCAM⁺) in the lungs of Fra-2^{ΔAlvII} mice (Supplemental Figure 3D). This is consistent with the limited expression of Fra-2 in SPC-positive cells after bleomycin (Figure 2, C and D) and confirms that SPC-Cre^{ERT2} does not target Fra-2-expressing hematopoietic cells (CD45⁺). Importantly, Fra-2^{ΔAlvII} mice and Fra-2-proficient littermates developed similar lung fibrosis upon bleomycin instillation with comparable sirius red positivity (Figure 3F), hydroxyproline accumulation (Figure 3G), and LR/DC ratio (Figure 3H). These data unequivocally demonstrate that Fra-2 expression in AEC2 cells is not required for lung fibrosis development and that the milder fibrosis observed in Fra-2^{ΔAd} mice is likely due to Fra-2 inactivation in nonepithelial cells.

Myeloid-specific Fra-2 inactivation reduces, while Fra-2^{fl/fl} BM potentiates, lung fibrosis. The constitutively expressed *Lyz2-Cre* knockin allele (34), also called *LysM*, was used to inactivate Fra-2 in the myeloid lineage (Figure 4A). Fra-2^{Δmac} mice were healthy, and flow cytometry analyses using the GFP reporter revealed efficient and exclusive recombination of the floxed Fra-2 allele in lung myeloid cells, both in homeostasis and upon

bleomycin administration. Increased Fra-2-reporter expression after bleomycin was observed in a large fraction of macrophages and a small fraction of eosinophils, while expression in neutrophils, monocytes, and alveolar macrophages was comparable to that in untreated Fra-2^{Δmac} mice (Supplemental Figure 4A). Efficient Fra-2 recombination was further confirmed by quantitative reverse-transcription PCR (qRT-PCR) analyses of sorted macrophages, with 85.6% reduction of Fra-2 mRNA in bleomycin-treated Fra-2^{Δmac} mice (Supplemental Figure 4B), and by immunoblot of lung extracts (Supplemental Figure 4C).

No significant differences in the total number of pulmonary myeloid cells were observed between Fra-2^{Δmac} and Fra-2^{fl/fl} mice 10 days after bleomycin treatment (Figure 4B), indicating that Fra-2 is not essential for the increase in myeloid cells during fibrosis. Lung vessel leakage during the acute inflammatory response to bleomycin was also not different between genotypes (Supplemental Figure 4D). However, bleomycin-treated Fra-2^{Δmac} mice developed significantly less severe lung fibrosis, with decreased sirius red positivity (Figure 4C), lower collagen packing density (Supplemental Figure 4E), and reduced lung hydroxyproline content in the lung (Figure 4D). As a result, pulmonary function was significantly improved in Fra-2^{Δmac} mice (Figure 4E). Saline-treated Fra-2^{Δmac} mice were comparable to saline-treated Fra-2^{fl/fl} mice in all measured fibrosis-related parameters (Figure 4, C-E), and myeloid-specific deletion of a single Fra-2 allele (Fra-2^{+/fl}; *LysM-Cre*⁺ mice: Fra-2^{+/Δmac}) was not sufficient to affect collagen accumulation (Figure 4D) or lung function (Supplemental Figure 4F), additionally ruling out that the changes observed in Fra-2^{Δmac} mice are due to the *Lyz2-Cre* allele. Detailed analyses further revealed decreased induction of ECM genes, such as *Col3a1* and *Fnl1* (encoding for fibronectin), and the ECM proteins procollagen type I and fibronectin in Fra-2^{Δmac} lungs (Supplemental Figure 4, G and H). Interestingly, while total lung mRNA expression of AAM marker genes was decreased 21 days after bleomycin in Fra-2^{Δmac} mice compared with Fra-2^{fl/fl} mice (Supplemental Figure 4I), no difference was observed between these 2 groups in lung macrophages sorted at day 14, except for *Nos2* (Figure 4F). *Arg1* was significantly upregulated after bleomycin compared with saline, but the increase was not affected by Fra-2 deletion (Figure 4F). These data indicate that, at least in the early phases of fibrosis, Fra-2 expression in myeloid cells is not crucial for the relative number or distribution of macrophage subpopulations or for the polarization of AAM, while it is essential to their fibrogenic activity in vivo.

BM transplantation experiments were next performed to assess whether increased Fra-2 expression in immune cells, particularly in the myeloid lineage, would potentiate fibrosis. WT or Fra-2^{Tg} BM was transplanted into lethally irradiated WT mice, which were subsequently subjected to bleomycin (Figure 4G). In this setting, no fibrosis was observed in the saline groups, and regardless of the BM genotype, a milder fibrosis developed 14 days after bleomycin, compared with our previous experiments using nontransplanted mice, in which fibrosis was severe. Importantly, mice reconstituted with Fra-2^{Tg} BM accumulated more collagen (Figure 4, H and I) and had worsened lung function (Figure 4J) after bleomycin treatment compared with mice transplanted with WT BM. This demonstrates that ectopic Fra-2 expression in immune cells promotes bleomycin-induced fibrosis.

Overall, these data strongly support an important functional contribution of Fra-2-expressing macrophages to lung fibrosis and suggest a crosstalk between activated macrophages recruited to the lung upon injury and ECM-producing cell types, such as pulmonary fibroblasts.

Macrophages release profibrotic factors in a Fra-2/AP-1-dependent manner. Monocyte-derived macrophages recruited to the lung are major contributors to murine lung fibrosis (35, 36). BM monocytes were therefore isolated from Fra-2^{Δmac} and Fra-2^{Tg} mice, differentiated into macrophages (BM-derived macrophages [BMDMs]), and assessed for their ability to induce a fibrogenic response in WT primary lung fibroblasts. BMDMs were differentiated and expanded using macrophage CSF-1 (MCSF-1) and either left untreated or exposed to the AAM-inducing cytokine IL-4 or to the AP-1 activity inhibitor T-5224 (37). Medium was next changed to serum- and factor-free medium, and the cells and their conditioned media (CM) were harvested 48 hours later (Figure 5A). IL-4 pretreatment increased Fra-2 mRNA expression in Fra-2^{fl/fl}, but not in Fra-2^{Δmac}, BMDMs (Figure 5B). Consistent with our in vivo observations, no difference in the expression of M(IL-4) marker genes was observed between the 2 genotypes (Supplemental Figure 5A), and the mRNA induction of *Tgfb1*, *Timp1*, and *Mmp12* in BMDMs was also comparable between genotypes (Supplemental Figure 5B). These data indicate that macrophage polarization in vitro in response to IL-4 is not substantially affected by Fra-2 inactivation. In an independent experiment, the Fra-2^{Δmac} BMDM expression of CAM markers in response to LPS was also largely comparable to that in WT, with the notable exception of higher *Il12a* induction (Supplemental Figure 5C).

Incubation of primary lung fibroblasts with CM from IL-4-pretreated BMDM increased cell viability independently of the BMDM genotype (Supplemental Figure 5D). However, increased mRNA expression of the myofibroblast markers *Acta2* and *Postn*, encoding α -SMA and periostin, respectively, was exclusively observed when lung fibroblasts were exposed to CM from IL-4-pretreated Fra-2-proficient BMDMs (Figure 5C). The reduced fibrogenic potential of Fra-2^{Δmac} BMDM CM compared with that in WT was also apparent by α -SMA immunoblot (Figure 5D). The profibrogenic activity of macrophages expressing Fra-2 was next assessed using nonpolarized Fra-2^{Tg} BMDMs treated with the AP-1 inhibitor T-5224 (38). Transgene expression was confirmed by qRT-PCR and GFP positivity (Figure 5E and data not shown). Interestingly, mRNA expression of

the M(IL-4) macrophage marker *Mrc1* was decreased in Fra-2^{Tg} BMDMs and only affected by T-5224 pretreatment in control BMDMs. *Chi3l3* (*Ym1*) tended to increase in Fra-2^{Tg} BMDMs, while the CAM marker *Il12a* was undetectable (Supplemental Figure 5E). Expression of *Tgfb1* and *Timp1* was not significantly altered, whereas increased *Mmp12* mRNA in Fra-2^{Tg} BMDMs was attenuated by T-5224 (Supplemental Figure 5F). Importantly, mirroring the Fra-2 loss-of-function setting, exposure to Fra-2^{Tg} BMDM CM induced fibrotic gene expression in lung fibroblasts, such as *Acta2*, which was prevented by AP-1 inhibitor pretreatment (Figure 5F). Collectively, these data indicate that in macrophages, Fra-2 controls the production of profibrogenic factors, but does not substantially alter their polarization.

ColVI chains are secreted by macrophages and are direct Fra-2 transcriptional targets. Macrophages are a major cellular component of the BALF in fibrotic mice (Supplemental Figure 2E), and exosomes often carry disease-specific proteins that could serve as biomarkers and therapeutic targets (39). We isolated exosomes from 2 experimental lung fibrosis paradigms, the spontaneous Fra-2^{Tg} and the bleomycin-induced WT mouse models, to find an unbiased representation of molecules secreted by cells in the local microenvironment of fibrotic lungs, including macrophages and possibly other cell types. Exosome-like vesicles were purified from the BALF of fibrotic Fra-2^{Tg} (12 weeks) and bleomycin-treated WT mice (12 days; Supplemental Figure 6A). NanoSight analyses revealed a reduced number of vesicles in both fibrosis models compared with nonfibrotic controls, while vesicles were larger in bleomycin-treated mice (Supplemental Figure 6B). Exosomal proteome was analyzed by label-free liquid chromatography–tandem mass spectrometry (LC-MS/MS), and around 400 proteins were identified in the BALF of WT mice with or without bleomycin, while more than 600 proteins were found in fibrotic Fra-2^{Tg} mice (Supplemental Figure 6C). Enrichment in extracellular- and vesicle-related protein profiles was confirmed by Gene Ontology analysis (Supplemental Figure 6D) with exosome markers, such as CD63, CD81, Alix, or Hsp90, present in all groups (data not shown). Importantly, the list of protein peptides identified in BALF exosomes from fibrotic, Fra-2^{Tg}, and bleomycin-treated WT mice, but not in healthy controls, was enriched in macrophage signatures (Supplemental Figure 6E), suggesting an increase of vesicles of myeloid origin during lung fibrosis. We next compared this list of exosome-derived potential fibrosis biomarkers to the genes found significantly changed in Fra-2^{Tg} prefibrotic lungs by RNA-Seq. Strikingly, peptides from all 3 ColVI chains, $\alpha 1$, $\alpha 2$, and $\alpha 3$, were present in BALF exosomes from fibrotic mice (Figure 6A and Supplemental Figure 6F), and their respective mRNAs, *Col6a1*, *Col6a2*, and *Col6a3*, were upregulated in prefibrotic Fra-2^{Tg} lungs (Supplemental Figure 6G). In the bleomycin model, *Col6a1*, *Col6a3*, and to a lesser extent, *Col6a2* mRNA were increased in the lungs of Fra-2^{fl/fl} mice at 21 days, but not in Fra-2^{Δmac} mice (Figure 6B). ColVI is a nonfibrillar collagen formed by trimers of $\alpha 1$, $\alpha 2$, and $\alpha 3$ chains that can promote fibroblast migration (40) and be secreted by macrophages (41). ColVI was coexpressed with Fra-2 in Ym1-positive, alternatively activated macrophages in fibrotic lungs of bleomycin-treated mice and also in fibrotic lungs sections of an independent experimental model of fibrosis (42), γ -herpesvirus-infected (MHV68) IFN- γ receptor KO (IFN γ R^{-/-}) mice (Supplemental Figure 6H). Additionally,

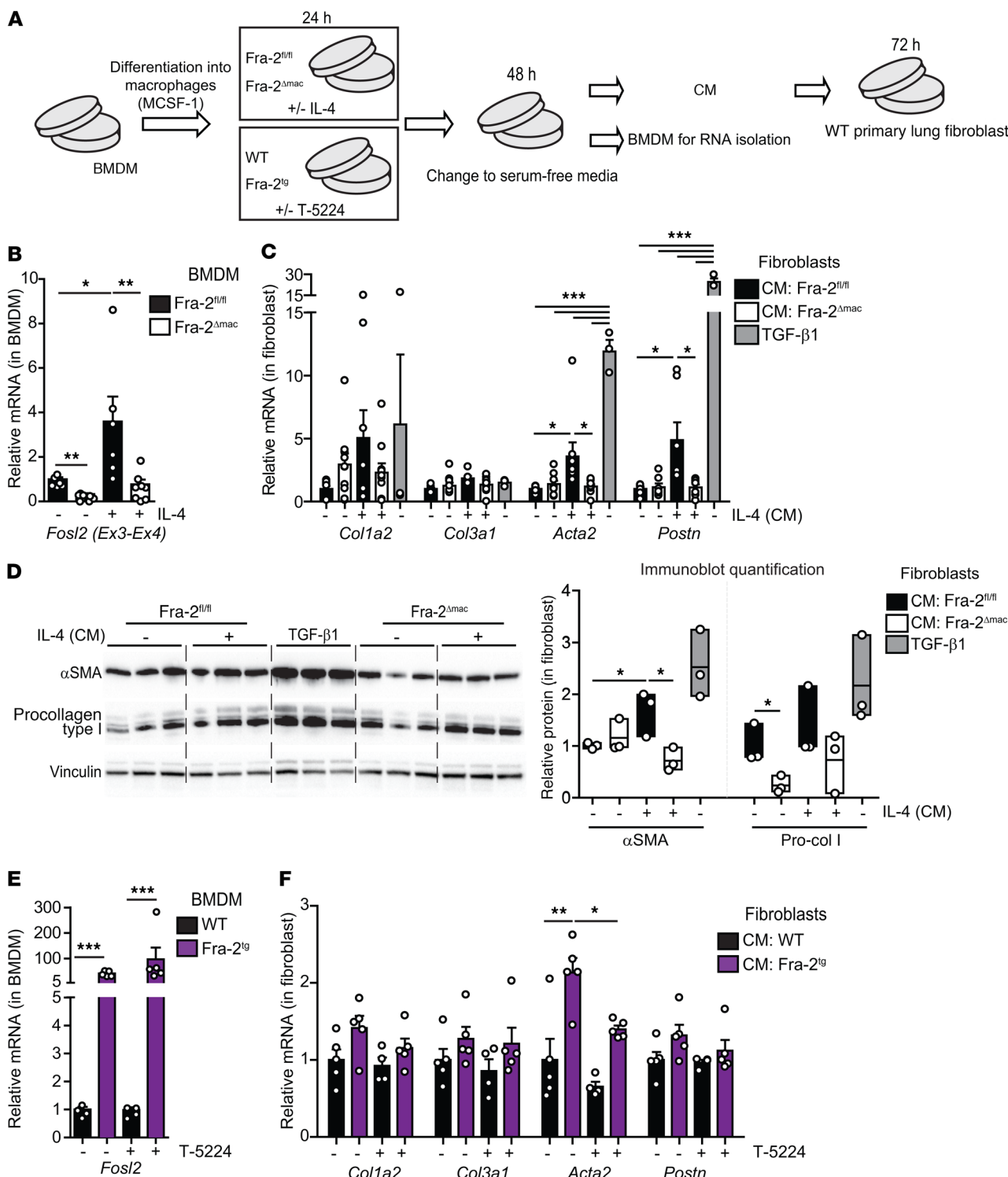


Figure 5. CM from Fra-2-expressing BM-derived macrophages induces lung fibroblast activation. (A) Experimental design to assess the effect of BMDM conditioned medium on WT primary lung fibroblasts. Experiment was repeated 5 and 2 times for the Fra-2 loss and gain of function, respectively. Each individual value represents a biological replicate, since each BMDM culture originates from 1 individual mouse. IL-4 was added at 20 ng/mL, T-5224 at 3 μM, and TGF-β1 at 0.5 ng/mL. (B) Fra-2 expression in BMDMs when CM was collected (qRT-PCR). Note that specific primers located in the floxed/deleted exons (Ex3-Ex4) are used. **P* < 0.05; ***P* < 0.01, 1-way ANOVA; Bonferroni's post test. (C) qRT-PCR analysis of fibroblast marker genes in primary WT lung fibroblasts cultured with CM and TGF-β1 (positive control). **P* < 0.05; ****P* < 0.001, 1-way ANOVA; Bonferroni's post test. Group analysis for each gene. TGF-β1, *n* = 3; other groups, *n* ≥ 7. (D) Immunoblot analysis of procollagen I and α-SMA in primary lung fibroblast lysates. Relative densitometry quantification for each protein is shown as a ratio to vinculin density (loading control). Individual values and mean ± SEM from 1 experiment are plotted. **P* < 0.05, unpaired *t* test; 1-tailed. Pro-coll I, procollagen I. (E) Fra-2 expression in WT and Fra-2^{Tg} BMDMs at the time the CM was collected (qRT-PCR). ****P* < 0.001, 1-way ANOVA; Bonferroni's post test. (F) qRT-PCR analysis of fibroblast marker genes in primary WT lung fibroblasts cultured with WT and Fra-2^{Tg} BMDM-CM. **P* < 0.05; ****P* < 0.01, paired 2-tailed *t* test. In all panels, bars represent mean ± SD/SEM. Relative mRNA and protein expression in untreated Fra-2^{fl/fl} BMDMs and derived CM is set to 1.

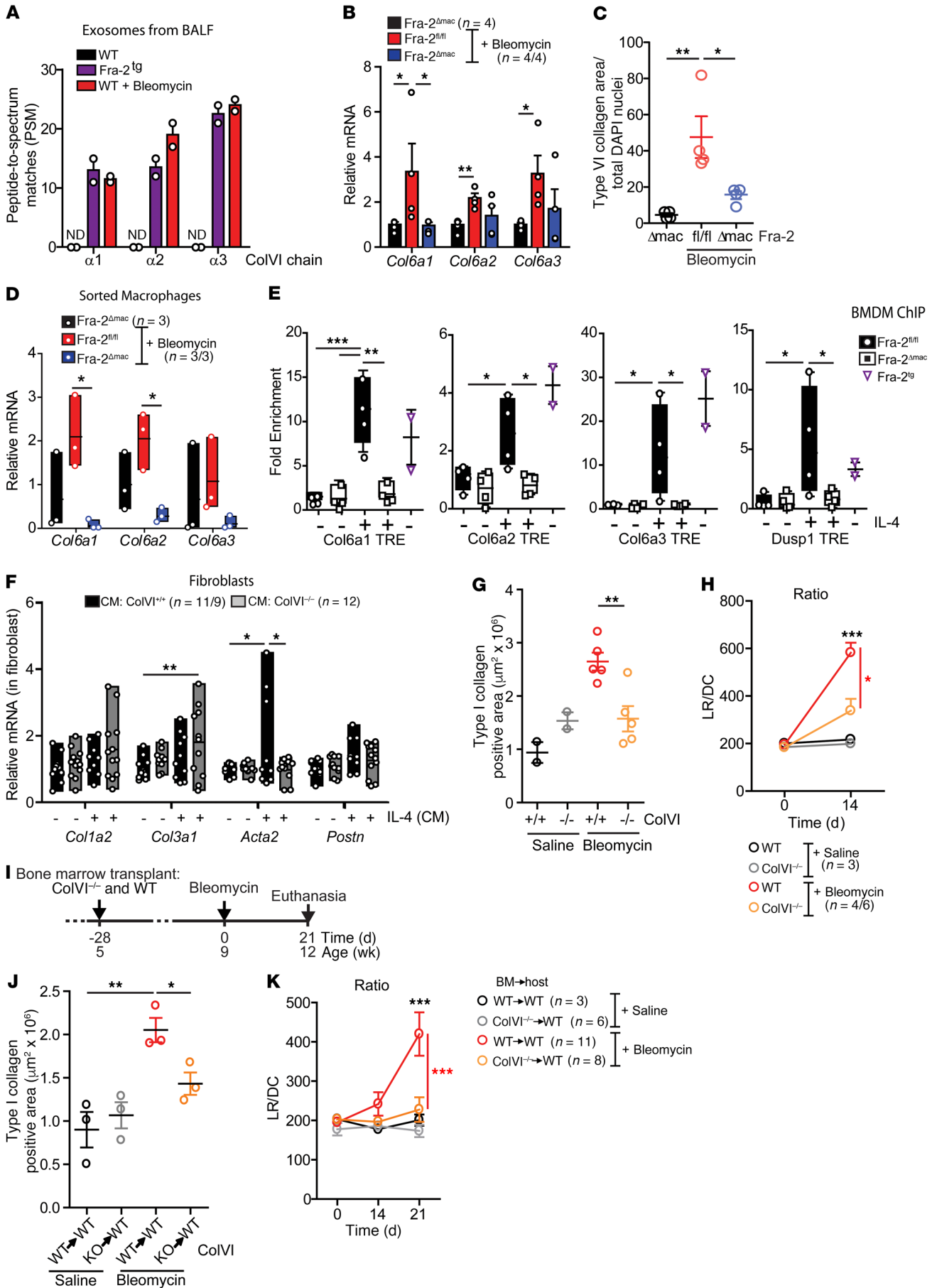


Figure 6. ColVI expression contributes to lung fibrosis. (A) Peptide-spectrum match (PSM) identified for ColVI fragments by LC-MS/MS of BALF exosomes extracted from 12-week-old WT mice, Fra-2^{Tg} mice, and WT mice after 12 days of bleomycin treatment. ND, not detected. (B) ColVI gene expression in lungs 21 days after treatment. Relative expression in saline-treated Fra-2^{fl/fl} is set to 1. **P* < 0.05; ***P* < 0.01, unpaired 1-tailed *t* test. (C) ColVI-positive area in lungs 21 days after treatment. Control group was treated with saline. Data were normalized to nuclei number. **P* < 0.05; ***P* < 0.01, 1-way ANOVA; Bonferroni's post test. (D) ColVI gene expression in sorted nonalveolar lung macrophages 14 days after bleomycin treatment. Expression in sorted cells from saline-treated lungs is set to 1. **P* < 0.05, unpaired 2-tailed *t* test. (E) Fra-2 ChIP assay in BMDM. Experiment was repeated twice. Relative expression in untreated Fra-2^{fl/fl} cells is set to 1. **P* < 0.05; ***P* < 0.01; ****P* < 0.001, unpaired 1-tailed *t* test. (F) Fibroblast marker gene expression in WT lung fibroblasts (CM, BMDM CM). Experiment was repeated twice. **P* < 0.05; ***P* < 0.01, 1-way ANOVA; Bonferroni's post test. (G) Type I collagen area of lungs 14 days after saline or bleomycin treatment. Data from 2 independent experiments are plotted. ***P* < 0.01, unpaired 2-tailed *t* test. (H) Respiratory function 14 days after saline or bleomycin treatment. Two independent sets of mice were treated. **P* < 0.05; ****P* < 0.001, 2-way ANOVA; Bonferroni's post test. (I) Schematic for experimental design and time line of saline- and bleomycin-treated WT mice transplanted with either WT BM (WT→WT) or ColVI^{-/-} BM (KO→WT). Bleomycin was injected into 2 independent sets of mice. (J) Type I collagen area at the end of the experiment. **P* < 0.05; ***P* < 0.01, unpaired 1-tailed *t* test. (K) Respiratory function 21 days after bleomycin. ****P* < 0.001, 2-way ANOVA; Bonferroni's post test.

ColVI protein expression in the lungs was significantly induced by bleomycin in WT mice compared with Fra-2^{Δmac} mice (Figure 6C) as well as in Fra-2^{Tg} BM chimeras compared with WT BM chimeras (Supplemental Figure 6I). Comparing *Col6a* gene expression in macrophages and mesenchymal and epithelial cells FACS sorted 14 days after bleomycin revealed that, although PDGFRα-positive mesenchymal cells have the highest relative ColVI expression when normalized to cell number, F4/80-positive macrophages are the only cell type in which the 3 ColVI genes are robustly induced by bleomycin (Supplemental Figure 7A). Furthermore, the increase in *Col6a* gene expression in lung macrophages FACS sorted 10 days after bleomycin (Figure 6D) or in IL-4-pretreated BMDMs (Supplemental Figure 7B) was largely Fra-2 dependent, as it was not observed in Fra-2^{Δmac} cells. Interestingly, Fra-2 did not appear to be essential for the *in vitro* induction of *Col6a* genes by TGF-β1 in primary lung (Supplemental Figure 7C) or embryonic (Supplemental Figure 7D) fibroblasts.

Collectively, these data indicate that, under fibrotic conditions, ColVI expression is increased in macrophages in 3 independent lung fibrosis paradigms in a Fra-2-dependent manner.

Inspection of the murine *Col6a* genes revealed several Fra-2/AP-1 dimer binding (TRE) elements in regulatory regions (Supplemental Figure 7E). ChIP-qPCR assays using *in vitro*-cultured BMDMs and specific Fra-2 antibodies demonstrated Fra-2 binding to TRE-containing promoter regions of *Col6a1*, *Col6a2*, and *Col6a3* in Fra-2^{Tg} and in Fra-2^{fl/fl} BMDMs pretreated with IL-4, but not in Fra-2-deficient BMDMs (Figure 6E), indicating that *Col6a* genes are direct Fra-2/AP-1 target genes in myeloid cells, implicated in the profibrogenic action of macrophages.

ColVI deficiency decreases fibrosis in vitro and in vivo. WT primary lung fibroblasts express higher *Acta2* when plated on ColVI (Supplemental Figure 8A). Primary lung fibroblasts exposed to CM from IL-4-pretreated *Col6a1*-KO (43) BMDMs (ColVI^{-/-}) failed to induce *Acta2* compared with WT BMDMs (Figure 6F), while M (IL-4) marker genes were similarly induced (Supplemental Figure 8B). Interestingly, CM from IL-4-treated ColVI^{-/-} BMDMs induced *Col3a1* mRNA in fibroblasts (Figure 6F), while the alterations in *Col1a2* mRNA and procollagen type I proteins were not significant (Figure 6F and Supplemental Figure 8C). Nevertheless, these *in vitro* data suggest that, similarly to what occurs in Fra-2-deficient cells, IL-4-polarization of ColVI-deficient macrophages is unaltered, while their profibrotic paracrine potential is impaired.

To evaluate the profibrotic role of ColVI *in vivo*, ColVI^{-/-} mice were subjected to the bleomycin lung fibrosis paradigm. qRT-PCR

analyses confirmed increased *Col6a1* gene expression in bleomycin-treated WT controls, which was undetectable in ColVI^{-/-} mutants (Supplemental Figure 8D). Importantly, while macrophage numbers were not overtly affected (data not shown), the ECM components type I collagen and fibronectin accumulated significantly less in ColVI-deficient lungs, and Fra-2 expression was reduced (Figure 6G and Supplemental Figure 8, E and F). Furthermore, lung function was significantly improved in ColVI-deficient mice 14 days after bleomycin (Figure 6H). We next treated lethally irradiated WT mice, reconstituted with either WT or ColVI-deficient BM, with bleomycin (Figure 6I and Supplemental Figure 8G). Mice transplanted with ColVI^{-/-} BM were protected from bleomycin-induced lung fibrosis compared with mice that received WT BM, with decreased type I collagen accumulation (Figure 6J), decreased sirius red positivity (Supplemental Figure 8H), and improved respiratory function 21 days after bleomycin treatment (Figure 6K). Taken together, these experiments clearly demonstrate a critical functional role of ColVI expression in immune cells, such as macrophages, during lung fibrosis.

Pharmacological AP-1 inhibition ameliorates fibrosis in the bleomycin model and in Fra-2^{Tg} mice. We next tested the therapeutic potential of the AP-1 inhibitor T-5224 (37). Saline- or bleomycin-treated WT mice were randomized at day 14, when the acute inflammation phase had subsided and fibrosis has developed, for daily T-5224 or vehicle (polyvinylpyrrolidone [PVP]) oral gavage over 1 week (Supplemental Figure 9A). Under these conditions and consistent with the previously reported benefits of T-5224 when supplied from day 10 (44), bleomycin-induced lung hydroxyproline was significantly lower in T-5224-treated mice than the vehicle-treated cohort (Supplemental Figure 9B). Pulmonary ColVI expression was also reduced (Supplemental Figure 9C), and most importantly, longitudinal plethysmography revealed a significant improvement in lung function with T-5224, with an LR/DC ratio almost reaching the values measured in mice that did not receive bleomycin (Supplemental Figure 9D).

We next treated 12-week-old already fibrotic Fra-2^{Tg} and WT littermates with T-5224 or PVP over 4 weeks (Figure 7A). As previously reported (38), extended T-5224 treatment was well tolerated and did not alter body weight (Supplemental Figure 9E). Importantly, T-5224 resulted in significantly less collagen accumulation in the lungs of Fra-2^{Tg} mice as measured at end point by sirius red positivity (Figure 7B and Supplemental Figure 9F) and hydroxyproline content (Figure 7C). Gene and protein analyses further confirmed ECM components, such as fibrillar collagens I and III

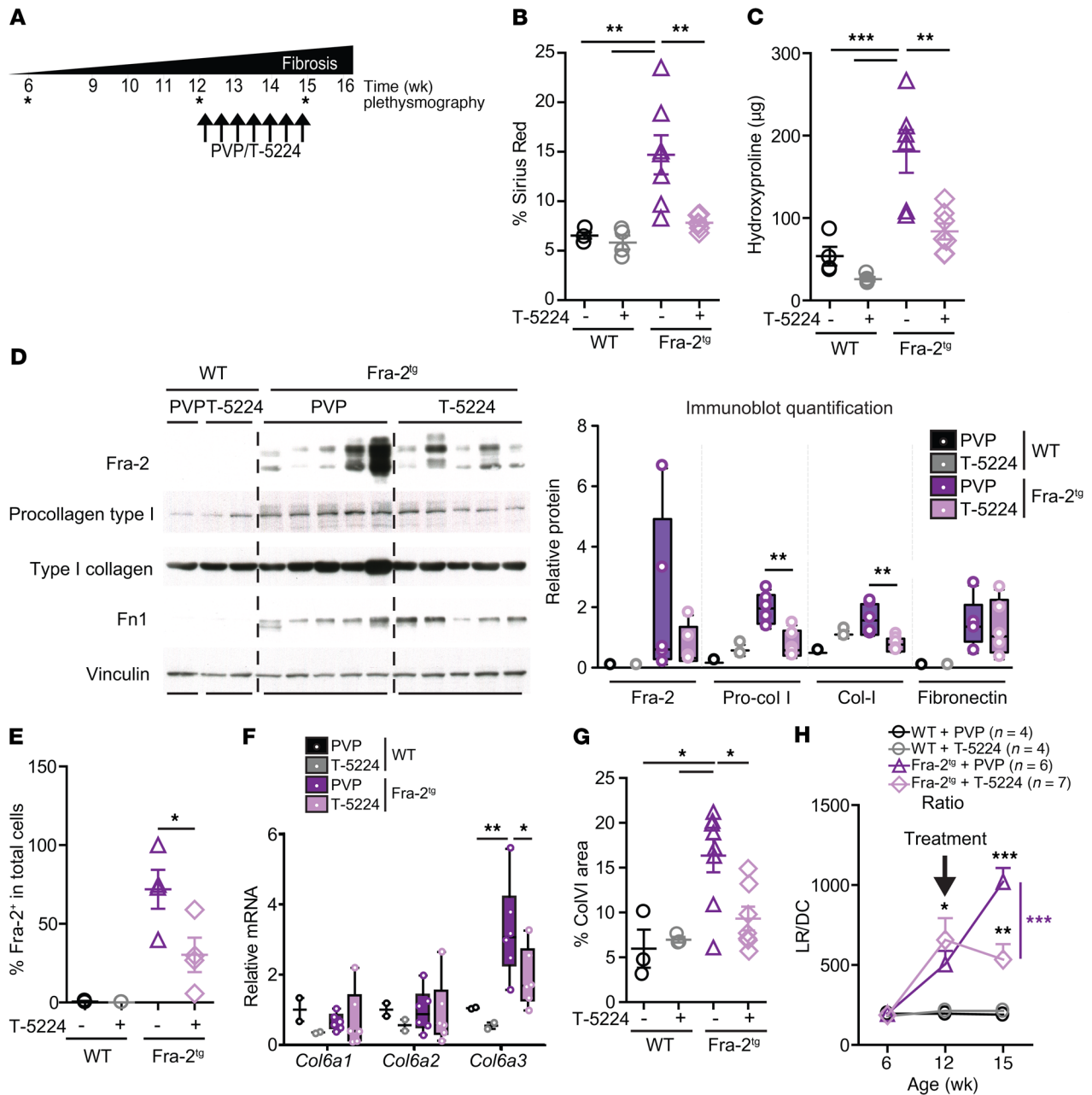


Figure 7. AP-1 inhibition reverts lung fibrosis in Fra-2^{tg} mice. (A) Schematic for AP-1 inhibitor T-5224 therapeutic protocol in Fra-2^{tg} mice. All data originate from 3 independent experiments designed as randomized blocks. Asterisks indicate when the plethysmography was performed within the experiment timeline. (B) Quantification of sirius red-positive areas in lungs at the end of the experiment. ***P* < 0.01, 1-way ANOVA; Bonferroni's post test. (C) Hydroxyproline content in lungs (left lobe). ****P* < 0.001, 1-way ANOVA; Bonferroni's post test. (D) Immunoblot analysis of Fra-2, procollagen I, type I collagen, and fibronectin in lung lysates at the end of the experiment. Band density quantification is shown in the graph, with individual values relative to vinculin (loading control). ***P* < 0.01, unpaired 2-tailed *t* test. (E) Quantification of Fra-2-positive nuclei in lung IF relative to total cells. **P* < 0.05, unpaired 2-tailed *t* test. (F) qRT-PCR analysis of ColVI genes in the lungs of Fra-2^{tg} and WT controls treated with T-5224 or PVP at the end of the experiment. Relative expression in WT+PVP is set to 1. **P* < 0.05; ***P* < 0.01, 1-way ANOVA; Bonferroni's post test. (G) Quantification of lung ColVI-positive area in IHC staining. **P* < 0.05, 1-way ANOVA; Bonferroni's post test. (H) Longitudinal analyses of respiratory function of Fra-2^{tg} and WT controls with T-5224 or vehicle. Note that the T-5224 or vehicle treatment started around 12 weeks of age, when animal respiratory function was already compromised (arrow). **P* < 0.05; ***P* < 0.01; ****P* < 0.001, 2-way ANOVA; Bonferroni's post test.

and fibronectin, were less expressed in the lungs of Fra-2^{tg} mice treated with T-5224 (Figure 7D and Supplemental Figure 9G). In T-5224-treated lungs, Fra-2 mRNA, protein, and the number of Fra-2-positive cells were decreased, while IL-4 appeared unaffected (Figure 7, D and E, and Supplemental Figure 9, H and I).

With the notable exception of decreased *Arg1* and *Nos2*, end-point mRNA expression of AAM and CAM marker genes was also minimally affected by T-5224 (Supplemental Figure 9J). Increased ColVI protein and *Col6a3* mRNA was still apparent in the lungs of Fra-2^{tg} mice at end-stage disease, but was attenuated by T-5224

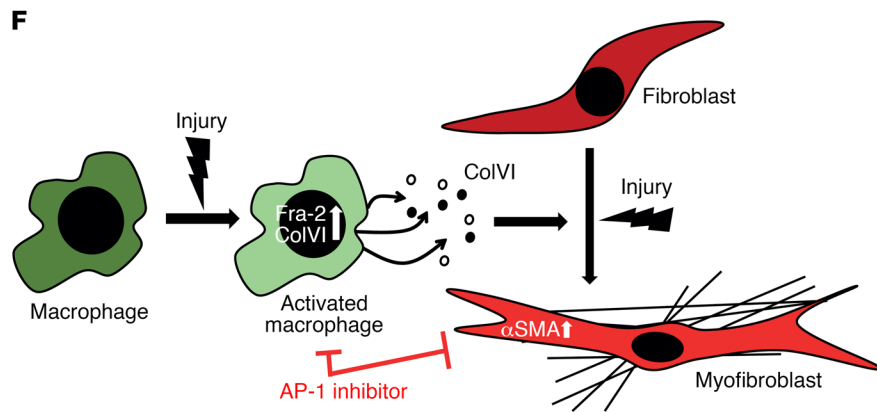
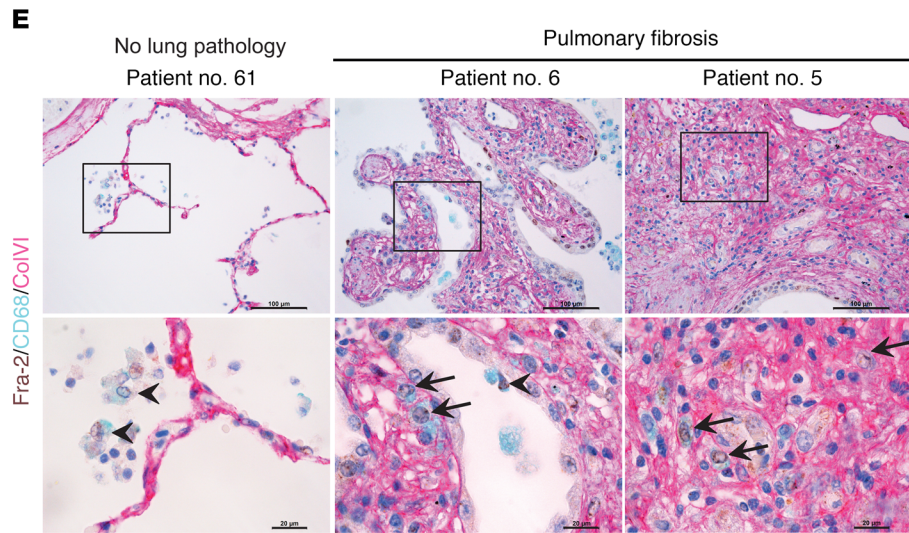
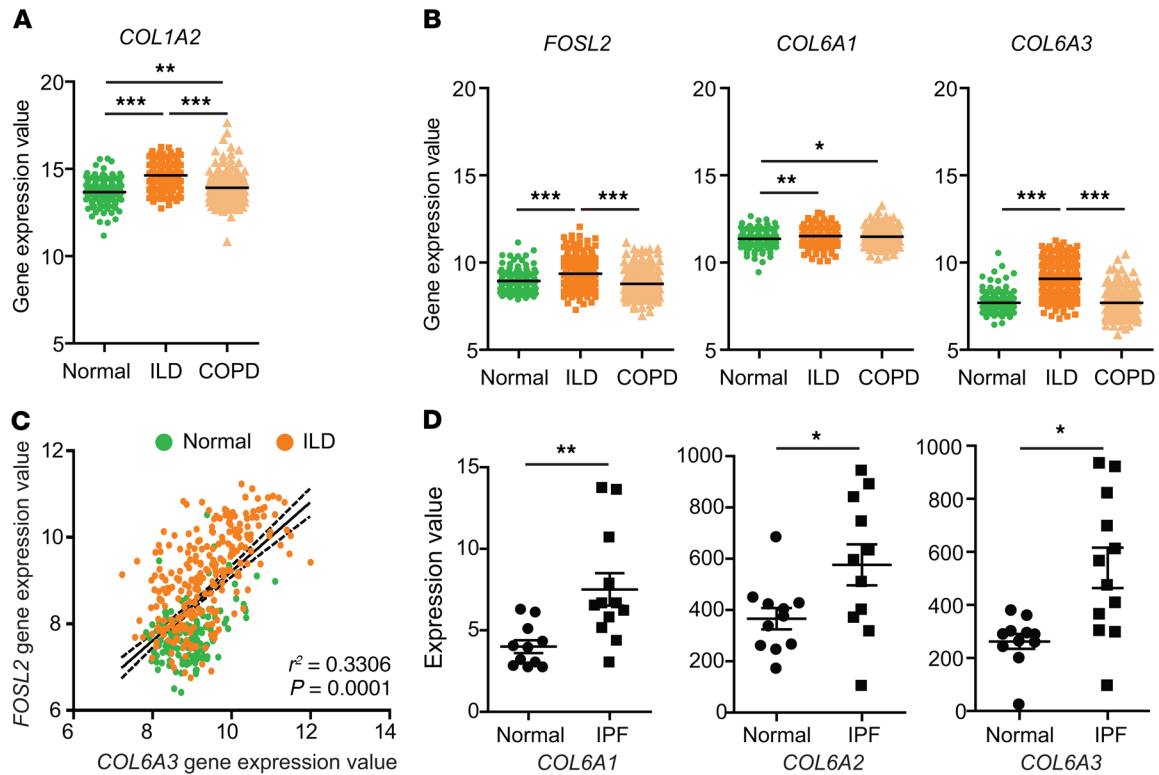


Figure 8. Fra-2 and ColVI expression in human lung fibrosis. (A) Gene expression values of *COL1A2* in lungs from human patients with normal histology (normal; $n = 173$) and diagnosed ILD ($n = 255$) and COPD ($n = 219$). Expression values were obtained from the public gene expression database of the LGRC (GSE47460). $**P < 0.01$; $***P < 0.001$, 1-way ANOVA; Bonferroni's post test. (B) Gene expression values of *FOSL2* (Fra-2), *COL6A1* (ColVI chain $\alpha 1$), and *COL6A3* (ColVI chain $\alpha 3$) genes in lungs from same cohort. Note that expression values for *COL6A2* (ColVI chain $\alpha 2$) were absent in the data set. $*P < 0.05$; $**P < 0.01$; $***P < 0.001$, 1-way ANOVA; Bonferroni's post test. (C) Expression values for *FOSL2* are plotted against *COL6A3* for linear regression and Pearson's correlation analysis of normal and ILD samples (r_2 and P values are indicated). (D) Gene expression values of ColVI genes in lungs from human patients with normal histology (normal) and diagnosed IPF. Expression values were obtained from a public curated data set (GDS1252). $*P < 0.05$; $**P < 0.01$, 2-tailed paired t test. (E) Triple IHC for Fra-2 (brown-nuclear), CD68 (blue-cytoplasmic), and ColVI (purple-extracellular) of human lungs from healthy and fibrosis patients. Nuclei are counterstained with hematoxylin. Arrows point to interstitial macrophages expressing Fra-2 and colocalizing with ColVI (triple positive); arrowheads point to Fra-2-positive alveolar macrophages. Scale bars: 100 μ m (low magnification); 20 μ m (high magnification). (F) Working model for the role of Fra-2/ColVI in macrophages during lung fibrosis.

treatment (Figure 7, F and G). Most strikingly, longitudinal plethysmography revealed a clear functional benefit of T-5224, as it halted the progressive decline in Fra-2^{tg} lungs. LR/DC remained stable in T-5224-treated mutants, while it further worsened in vehicle-treated Fra-2^{tg} mice (Figure 7H). These data demonstrate that lung fibrosis is substantially ameliorated by therapeutic AP-1 inhibition in 2 experimental models of fibrosis and that AP-1 pharmacological inhibitors such as T-5224 should therefore be considered for lung fibrosis therapy.

ColVI and Fra-2 are coexpressed in human fibrotic lungs and macrophages. Finally, we assessed Fra-2 and collagen gene expression in human disease by computational analysis of the Lung Genomics Research Consortium (LGR) database, with gene expression data from diseased lung tissue from 255 ILD and 219 chronic obstructive pulmonary disease (COPD) patients and normal lung tissue from 173 thoracic surgery patients (GSE47460). The fibrosis marker *COL1A2* (type I collagen) was increased in both diseased cohorts (Figure 8A). Importantly, while *COL6A1* was higher in patients with both ILD and COPD compared with healthy individuals, *FOSL2* and *COL6A3* were specifically increased in ILD samples, but not in COPD samples (Figure 8B). Increased FRA-2 and COLVI were observed in lung protein extracts from an independent patient cohort (data not shown). Furthermore, the expression of *FOSL2* and *COL6A3* positively correlated across ILD and healthy samples (Figure 8C). A similar analysis using an independent data set for IPF (GDS1252) also showed increased mRNA expression of *COL6A1* and *COL6A3* and indicated that *COL6A2* is also increased in IPF lung samples compared with healthy lungs (Figure 8D and ref. 45). Importantly, both alveolar and interstitial macrophages highly express Fra-2 in lung sections from fibrosis patients when compared with healthy tissues. Furthermore, Fra-2, ColVI, and CD68 (human macrophage marker) triple immunohistochemistry indicated that interstitial macrophages expressing Fra-2 also express ColVI (Figure 8E). These results indicate that Fra-2 expression in AAMs contributes to mouse and human lung fibrosis, possibly by controlling the expression of secreted factors, such as ColVI.

Discussion

The role of the immune response in lung fibrosis and its potential as therapeutic target are not clearly established. Here, we provide evidence for a functional contribution of Fra-2-expressing macrophages to the paracrine activation of fibroblasts and to lung fibrosis (Figure 8F). We identify ColVI as a Fra-2 transcriptional target in macrophages and unravel a profibrogenic role for ColVI in vitro and in vivo. Importantly, inhibiting Fra-2/AP-1 or ColVI is therapeutically relevant in mouse models of lung fibrosis.

The fibrotic phenotype in the Fra-2^{tg} model of fibrosis is reminiscent of a type 2 cytokine-driven disease with enhanced IL-4 expression, IL-4 pathway signature, eosinophil/neutrophil infiltration, and M(IL-4) macrophage enrichment (25, 28, 46). The contribution of type 2 cytokines, IL-4 and IL-13, to macrophage activation and fibrosis development in different organs is well accepted (4, 47, 48). Lung-specific expression of these cytokines increases after bleomycin treatment, although their importance in this particular lung fibrosis model is controversial (49–51). While type 2 cytokines seem dispensable or even

detrimental in the early phases after bleomycin treatment, these likely promote subsequent fibrotic events (52, 53). IL-4 and IL-13 induce Fra-2 expression in macrophages (ref. 54 and our in vitro data) and promote profibrotic macrophage activation and myofibroblast differentiation (14, 55, 56). We demonstrate that Fra-2 expression in macrophages is not essential for the early inflammatory phase of bleomycin-induced fibrosis nor for macrophage recruitment or phenotypic switch, but modulates the expression of molecules produced by M(IL-4) macrophages to promote the differentiation of fibroblasts to myofibroblasts and lung fibrosis. This is particularly relevant, as clinical trials for IPF and other type 2 immunity diseases using blocking antibodies against type 2 cytokines had limited success, likely due to exacerbation of type 1 (Th1) inflammation or impaired tissue regeneration (57, 58). New strategies decreasing the profibrotic arm of type 2 (Th2) inflammation and/or targeting AAMs secretory/paracrine activity without affecting tissue repair and Th1 inflammation are therefore urgently needed.

Macrophage-secreted factors, such as platelet-derived growth factor (PDGF), TGF- β 1, MMPs, and tissue-inhibitor metalloproteinases (TIMPs), can induce and sustain fibroblast-to-myofibroblast activation (59–63). This and the recently proposed direct transition from macrophages to myofibroblasts (64) defines the current understanding of macrophage-fibroblast crosstalk in wound healing and fibrosis. PDGF and TGF- β signaling modulate vascular remodeling in Fra-2^{tg} mice, but appear largely dispensable for lung fibrogenesis (28, 65). No MMPs/TIMPs were found consistently deregulated in the lung, macrophage, and/or BMDM cultures across the different experimental models used in the current study. Instead, we unraveled an important contribution of ColVI, a direct transcriptional target of Fra-2/AP-1 in macrophages, in modulating fibroblast activation in vitro and fibrogenesis in vivo. We provide experimental evidence for this Fra-2/ColVI connection in 3 independent experimental models of lung fibrosis — chemical, virus, and transgene induced (25, 42, 66) — as well as in patient samples. In the bleomycin model, we show for what we believe is the first time that ectopic Fra-2 expression in BM promotes lung fibrosis, while myeloid-specific Fra-2 inactivation as well as complete or BM-derived ColVI deficiency is protective. While the contribution of other BM-derived cell types cannot be excluded in the transplantation experiments, our collective data in vitro and in vivo suggest that monocyte/macrophages expressing Fra-2 are a relevant functional source of profibrotic ColVI. A more definitive assessment of the contribution of ColVI-expressing macrophages in vivo would require the generation of a new mouse model with conditional ColVI alleles and/or efficient and long-term engraftment of adoptively transferred ColVI-deficient monocytes. Both experimental strategies are challenging and time consuming. As Fra-2 and ColVI are broadly expressed in other fibrosis-relevant lung cell types, such as in mesenchymal cells, future investigations using the appropriate cell-specific genetic tools are certainly warranted for exploring and fully determining the functional role of these 2 genes in the lung and also in tissue fibrosis.

Monocyte-derived macrophages are key drivers of lung fibrosis, replenishing alveolar macrophages immediately lost upon injury (35, 36, 67). While macrophage depletion during wound healing resulted in antagonistic phase-dependent outcomes (68), it

prevented fibrosis in several models (69, 70), including bleomycin-induced lung fibrosis (11, 63, 71, 72). Nintedanib, the first-line treatment for IPF, is a potent inhibitor of several growth factor receptors, including the macrophage-survival cytokine M-CSF-R. Nintedanib reduces circulating M-CSF and skin AAMs in Fra-2^{Tg} mice and ameliorates skin and lung fibrosis (46). ColVI expression by macrophages promotes lung fibroblast activation, but similarly to Fra-2, is not essential for the macrophage phenotype switch. Consistent with the implication of AP-1 proteins Fra-2 and c-Jun and the AP-1-activating JNK kinases in lung fibrosis (73, 74), pharmacological AP-1 inhibition decreased ColVI expression and substantially ameliorated bleomycin- and Fra-2^{Tg}-induced fibrosis. Therefore, unlike conventional strategies aiming at depleting macrophages or blocking IL-4/IL13/Th2 response, the more restricted outcome of targeting Fra-2/ColVI using compounds such as T-5224 would provide a therapeutic opportunity to block the profibrogenic arm of chronic Th2-associated diseases without affecting proregenerative effectors.

Increased ColVI in IPF patient lung sections was reported (75). We now show that Fra-2 and ColVI are coexpressed in human IPF lung macrophages and specifically increased and correlated in ILD, but not inflammatory COPD, indicating that coexpression of Fra-2 and ColVI could be a better biomarker for lung fibrosis than type I collagen, which is increased in both diseases. Whether, similarly to what occurs with Fra2^{Tg} and bleomycin-treated mice, ColVI peptides are detectable in BALF exosome-like vesicles from IPF patients undergoing diagnostic bronchoscopy awaits experimental evaluation. In conclusion, Fra-2-expressing macrophages and ColVI are two therapeutically relevant determinants of paracrine fibroblast activation and tissue fibrogenesis. Further work will likely identify additional Fra-2/AP-1-regulated molecules that could be targeted therapeutically and stimulate the development of specific drugs for these largely untreatable human diseases.

Methods

Mouse procedures. *H2kb-fosl2-LTR*, *Lyz2-Cre*, *sftpc-CreERT2*, *col6a1^{KO}*, and *fosl2^d* alleles are described elsewhere (25, 31, 43, 76). All mouse lines were maintained on a C57BL/6 background and housed in a specific pathogen-free facility accredited by the American Association for Laboratory Animal Care (AALAC), with food and water ad libitum. Male mice were anesthetized by i.p. injection of medetomidine (Domtor) and ketamine (Imalgene), intubated with a 24-gauge catheter (BD), and instilled with a single dose of 1.5 U/kg of bleomycin (MilliporeSigma). Anesthesia was reverted with atipamezole (Antisedan) and mice euthanized at different time points using carbon dioxide. Bleomycin-treated and Fra-2^{Tg} mice were monitored by body weight control and lung mechanics measurement (plethysmography). When indicated, 2.5×10^8 PFU of either Cre-expressing, GFP-expressing, or empty adenovirus were delivered intratracheally after anesthesia. Tamoxifen was injected i.p. (10 mg/d) for 5 consecutive days to trigger Cre recombinase activity in Fra-2^{AAV1} mice. At the experimental end point, blood was collected by cardiac puncture after euthanasia. In all experiments, sex-matched littermates were used as controls. IFN γ ^{R-/-} C57BL/6 mice were bred in house. Gamma-herpes virus-induced lung fibrosis was performed as previously described (42). In brief, mice were infected at 8 to 12 weeks of age. Prior to infection,

mice were sedated with isoflurane and intranasally infected with 5×10^5 PFU in 20 μ l of DMEM. For the transplantation experiments, lethally irradiated WT mice (14 Gy) were transplanted i.v. with 2×10^6 BM cells from donor mice.

Lung plethysmography. Mice were anesthetized by i.p. injection of medetomidine (Domtor) and ketamine (Imalgene, Merial Laboratories), intubated with a 24-gauge catheter (BD), and introduced in the chamber of a plethysmograph (EMKA). A MiniVent (Harvard Apparatus) was connected to the plethysmograph and the tracheal cannula for animal ventilation at 10 ml/kg of tidal volume and 150 breaths per minute. Data were measured by 2 pressure transducers that detect pressure variations in the chamber (flow) and in the tracheal cannula (pressure). This allows for measurements of LR (mmHg/mL \times s⁻¹) and DC (mL/mmHg) in addition to other lung function parameters. Lung function measurement was repeated at least 3 times and the data averaged for each mouse. Fibrotic lungs show increased LR and decreased DC (reduced tissue elasticity).

Cell culture. Primary mouse lung fibroblasts were isolated from adult mice. Lungs were perfused with saline to eliminate blood cells and lung tissue was minced and incubated for 45 minutes in serum-free media with 0.14 Wunsch units/mL Liberase Blendzyme 3 (Roche). After centrifugation, the pellet was resuspended in 20% FBS and 1% penicillin-streptomycin-supplemented DMEM/F12 culture media (Lonza). Cells attaching from the tissue pieces were trypsinized and cultured in monolayer. When confluent, CD45-negative cells were sorted to purify the cell culture from possible hematopoietic cell contamination. All lung fibroblasts were used between passages 3 and 5.

Primary BMDMs were isolated from adult mice by differentiation of BM-derived monocytes with incubation of 3 to 5 days with 50 ng/mL of mouse MCSF-1 (R&D and Preprotech) in bacteria plates. Before confluence, cells were trypsinized, counted, and plated again at a similar number for the experiments. Mouse IL-4 (Preprotech) was added at a concentration of 20 ng/mL, while the AP-1 inhibitor T-5224 was added at 3 μ M. LPS was added at 1 μ g/mL. For CM experiments, cells were cultured in serum- and phenol red-free media. When collected, supernatants were centrifuged, filtered through a 45 μ m filter, and aliquoted before storage. Fibronectin, ColII, and ColVI were used to precoat culture dishes (20 μ g/mL). Primary lung fibroblasts were harvested for RNA analysis 24 hours after plating. Fra-2^{Tg} mouse lung RNA-Seq data were deposited in the NCBI's Gene Expression Omnibus database (GEO GSE103355).

For further information, see Supplemental Methods. See complete unedited blots in the supplemental material.

Statistics. Unless otherwise specified, data are expressed as mean \pm SEM and individual values are plotted. Statistical significance was determined using either paired or unpaired *t* test (1 or 2 tailed) or Mann-Whitney *U* test according to sample distribution for comparing 2 groups of samples. One-way ANOVA or two-way ANOVA was performed for grouped or multivariate analysis, as appropriate. For all experiments, *P* < 0.05 was considered statistically significant.

Study approval. All animal studies were approved by the CNIO IACUC, by the ethics and animal welfare committee of the the Instituto de Salud Carlos III (Madrid, Spain) and by the Comunidad de Madrid (Madrid, Spain), in accordance with National and European regulations. In the case of the MHV68-induced lung fibrosis mouse model, the protocol was approved by the Emory University Institutional Animal Care and Use Committee and in accordance with established guidelines and policies at Emory University School of Medicine (pro-

tolocol YER-2002245-031416GN). The protocol was also carried out in strict accordance with the recommendations in the *Guide for the Care and Use of Laboratory Animals* (National Academies Press, 2011). The project design to obtain human samples was approved by the ethical committee of the Instituto de Salud Carlos III (Madrid, Spain). In addition, samples and/or data from patients included in this study were provided by the Biobanco i+12 in the Hospital 12 de Octubre integrated in the Spanish Hospital Biobanks Network (RetBioH; www.redbiobancos.es) following standard operation procedures, with appropriate approval of the Ethical and Scientific Committees, Madrid Spain. Paraffin-embedded tissue sections and OCT-embedded fresh tissue from 11 pulmonary fibrosis patients and 3 controls without any lung pathology were obtained. All patients provided informed consent.

Author contributions

ACU designed and performed experiments and wrote the paper. LB contributed to mouse colony management, experimental design, and manuscript writing. MS contributed to experimental design and provided the data for the bleomycin experiment in WT mice. BR designed and analyzed flow cytometry experiments and contributed to manuscript writing. MJ contributed to experimental design and performed some of the experiments. CFT analyzed the RNA-Seq data. PXE acquired and analyzed LC-MS/MS data. AIH synthesized the T-5224 inhibitor. DM acquired and analyzed confocal microscopy images. P Braghetta and P Bonaldo provided the ColVI-deficient mice and bones for in vitro and in vivo experiments. PM provided data and samples from the MVH68 model.

LPA provided access to the human lung samples. EFW directed the study, approved the data, and edited the paper.

Acknowledgments

We thank Brigid L.M. Hogan, Irmgard Förster, and Harold L. Moses for the *Sftpc-CreERT2*, *Lys2-Cre*, and *S100a4-Cre* mouse lines and Chiara Cianciaruso and Dario Bizzotto for helping with the ColVI-deficient samples and mice. We are grateful to the members of the Wagner laboratory for valuable suggestions; V. Bermeo and F. Montes for technical help; S. Leceta, G. Medrano, and P. García for assisting with mouse experiments, and the staff at the Histopathology Unit at CNIO for optimizing triple human IHC. We are thankful to the Biobanco i+12 at the Hospital 12 de Octubre, integrated in the Spanish Hospital Biobanks Network (RetBioH) and supported by the Instituto de Salud Carlos III, to Ana Belén Enguita for human samples selection, and above all, to the patients for informed consent. The EFW laboratory is supported by grants from the Spanish Ministry of Economy (BFU2012-40230 and SAF2015-70857), cofunded by the ERDF-EU, the Daiichi Sankyo Company, and a Jesus Serra Visiting Scientist Grant to Wolfgang Weninger/BR.

Address correspondence to: Erwin F. Wagner, Department of Dermatology and Department of Laboratory Medicine, Medical University of Vienna, Lazarettgasse 14a, A-1090 Vienna, Austria. Phone: 43.1.40400.73506; Email: erwin.wagner@meduniwien.ac.at.

- Zeisberg M, Kalluri R. Cellular mechanisms of tissue fibrosis. 1. Common and organ-specific mechanisms associated with tissue fibrosis. *Am J Physiol, Cell Physiol.* 2013;304(3):C216–C225.
- Bonnans C, Chou J, Werb Z. Remodelling the extracellular matrix in development and disease. *Nat Rev Mol Cell Biol.* 2014;15(12):786–801.
- Richeldi L. Idiopathic pulmonary fibrosis: moving forward. *BMC Med.* 2015;13:231.
- Gieseck RL, Wilson MS, Wynn TA. Type 2 immunity in tissue repair and fibrosis. *Nat Rev Immunol.* 2018;18(1):62–76.
- Ley B, Collard HR, King TE. Clinical course and prediction of survival in idiopathic pulmonary fibrosis. *Am J Respir Crit Care Med.* 2011;183(4):431–440.
- Richeldi L, et al. Efficacy and safety of nintedanib in idiopathic pulmonary fibrosis. *N Engl J Med.* 2014;370(22):2071–2082.
- Noble PW, et al. Pirfenidone in patients with idiopathic pulmonary fibrosis (CAPACITY): two randomised trials. *Lancet.* 2011;377(9779):1760–1769.
- Luppi F, Cerri S, Beghè B, Fabbri LM, Richeldi L. Corticosteroid and immunomodulatory agents in idiopathic pulmonary fibrosis. *Respir Med.* 2004;98(11):1035–1044.
- Wuyts WA, et al. The pathogenesis of pulmonary fibrosis: a moving target. *Eur Respir J.* 2013;41(5):1207–1218.
- Balestro E, et al. Immune inflammation and disease progression in idiopathic pulmonary fibrosis. *PLoS ONE.* 2016;11(5):e0154516.
- Gibbons MA, et al. Ly6Chi monocytes direct alternatively activated profibrotic macrophage regulation of lung fibrosis. *Am J Respir Crit Care Med.* 2011;184(5):569–581.
- Wynn TA, Barron L. Macrophages: master regulators of inflammation and fibrosis. *Semin Liver Dis.* 2010;30(3):245–257.
- Murray PJ, Wynn TA. Protective and pathogenic functions of macrophage subsets. *Nat Rev Immunol.* 2011;11(11):723–737.
- Van Linthout S, Miteva K, Tschöpe C. Crosstalk between fibroblasts and inflammatory cells. *Cardiovasc Res.* 2014;102(2):258–269.
- Nucera S, Biziato D, De Palma M. The interplay between macrophages and angiogenesis in development, tissue injury and regeneration. *Int J Dev Biol.* 2011;55(4–5):495–503.
- Vannella KM, Wynn TA. Mechanisms of organ injury and repair by macrophages. *Annu Rev Physiol.* 2017;79:593–617.
- Yamauchi K, Martinet Y, Crystal RG. Modulation of fibronectin gene expression in human mononuclear phagocytes. *J Clin Invest.* 1987;80(6):1720–1727.
- Larson-Casey JL, Deshane JS, Ryan AJ, Thannickal VJ, Carter AB. Macrophage Akt1 kinase-mediated mitophagy modulates apoptosis resistance and pulmonary fibrosis. *Immunity.* 2016;44(3):582–596.
- Pyonteck SM, et al. CSF-1R inhibition alters macrophage polarization and blocks glioma progression. *Nat Med.* 2013;19(10):1264–1272.
- Gordon S, Martinez FO. Alternative activation of macrophages: mechanism and functions. *Immunity.* 2010;32(5):593–604.
- Kaviratne M, et al. IL-13 activates a mechanism of tissue fibrosis that is completely TGF-beta independent. *J Immunol.* 2004;173(6):4020–4029.
- Doucet C, Brouty-Boyd D, Pottin-Clémenceau C, Canonica GW, Jasmin C, Azzarone B. Interleukin (IL) 4 and IL-13 act on human lung fibroblasts. Implication in asthma. *J Clin Invest.* 1998;101(10):2129–2139.
- Zenz R, et al. Psoriasis-like skin disease and arthritis caused by inducible epidermal deletion of Jun proteins. *Nature.* 2005;437(7057):369–375.
- Eferl R, Wagner EF. AP-1: a double-edged sword in tumorigenesis. *Nat Rev Cancer.* 2003;3(11):859–868.
- Eferl R, et al. Development of pulmonary fibrosis through a pathway involving the transcription factor Fra-2/AP-1. *Proc Natl Acad Sci U S A.* 2008;105(30):10525–10530.
- Sisson TH, et al. Targeted injury of type II alveolar epithelial cells induces pulmonary fibrosis. *Am J Respir Crit Care Med.* 2010;181(3):254–263.
- Barkauskas CE, et al. Type 2 alveolar cells are stem cells in adult lung. *J Clin Invest.* 2013;123(7):3025–3036.
- Tsujino K, Reed NI, Atakilit A, Ren X, Sheppard D. Transforming growth factor-β plays divergent roles in modulating vascular remodeling, inflammation, and pulmonary fibrosis in a murine model of scleroderma. *Am J Physiol Lung Cell Mol Physiol.* 2017;312(1):L22–L31.
- Murray PJ, et al. Macrophage activation and polarization: nomenclature and experimental guidelines. *Immunity.* 2014;41(1):14–20.
- Peng R, et al. Bleomycin induces molecular changes directly relevant to idiopathic pulmo-

- nary fibrosis: a model for “active” disease. *PLoS ONE*. 2013;8(4):e59348.
31. Eferl R, Zenz R, Theussl HC, Wagner EF. Simultaneous generation of fra-2 conditional and fra-2 knock-out mice. *Genesis*. 2007;45(7):447–451.
 32. Sutherland KD, Song JY, Kwon MC, Proost N, Zevenhoven J, Berns A. Multiple cells-of-origin of mutant K-Ras-induced mouse lung adenocarcinoma. *Proc Natl Acad Sci U S A*. 2014;111(13):4952–4957.
 33. Rock JR, et al. Multiple stromal populations contribute to pulmonary fibrosis without evidence for epithelial to mesenchymal transition. *Proc Natl Acad Sci U S A*. 2011;108(52):E1475–E1483.
 34. Clausen BE, Burkhardt C, Reith W, Renkawitz R, Förster I. Conditional gene targeting in macrophages and granulocytes using LysMcre mice. *Transgenic Res*. 1999;8(4):265–277.
 35. Satoh T, et al. Identification of an atypical monocyte and committed progenitor involved in fibrosis. *Nature*. 2017;541(7635):96–101.
 36. Misharin AV, et al. Monocyte-derived alveolar macrophages drive lung fibrosis and persist in the lung over the life span. *J Exp Med*. 2017;214(8):2387–2404.
 37. Tsuchida K, et al. Design, synthesis, and biological evaluation of new cyclic disulfide decapeptides that inhibit the binding of AP-1 to DNA. *J Med Chem*. 2004;47(17):4239–4246.
 38. Aikawa Y, et al. Treatment of arthritis with a selective inhibitor of c-Fos/activator protein-1. *Nat Biotechnol*. 2008;26(7):817–823.
 39. Skog J, et al. Glioblastoma microvesicles transport RNA and proteins that promote tumour growth and provide diagnostic biomarkers. *Nat Cell Biol*. 2008;10(12):1470–1476.
 40. Knüppel L, et al. FK506-binding protein 10 (FKBP10) regulates lung fibroblast migration via collagen VI synthesis. *Respir Res*. 2018;19(1):67.
 41. Schnoor M, et al. Production of type VI collagen by human macrophages: a new dimension in macrophage functional heterogeneity. *J Immunol*. 2008;180(8):5707–5719.
 42. O’Flaherty BM, et al. CD8+ T cell response to gammaherpesvirus infection mediates inflammation and fibrosis in interferon gamma receptor-deficient mice. *PLoS ONE*. 2015;10(8):e0135719.
 43. Bonaldo P, Braghetta P, Zanetti M, Piccolo S, Volpin D, Bressan GM. Collagen VI deficiency induces early onset myopathy in the mouse: an animal model for Bethlem myopathy. *Hum Mol Genet*. 1998;7(13):2135–2140.
 44. Chen H, et al. Mechanosensing by the $\alpha 6$ -integrin confers an invasive fibroblast phenotype and mediates lung fibrosis. *Nat Commun*. 2016;7:12564.
 45. Pardo A, et al. Up-regulation and profibrotic role of osteopontin in human idiopathic pulmonary fibrosis. *PLoS Med*. 2005;2(9):e251.
 46. Huang J, et al. Nintedanib inhibits macrophage activation and ameliorates vascular and fibrotic manifestations in the Fra2 mouse model of systemic sclerosis. *Ann Rheum Dis*. 2017;76(11):1941–1948.
 47. Wynn TA. Type 2 cytokines: mechanisms and therapeutic strategies. *Nat Rev Immunol*. 2015;15(5):271–282.
 48. Vannella KM, et al. Combinatorial targeting of TSLP, IL-25, and IL-33 in type 2 cytokine-driven inflammation and fibrosis. *Sci Transl Med*. 2016;8(337):337ra65.
 49. Wilson MS, et al. Bleomycin and IL-1beta-mediated pulmonary fibrosis is IL-17A dependent. *J Exp Med*. 2010;207(3):535–552.
 50. Jakubzick C, et al. The therapeutic attenuation of pulmonary fibrosis via targeting of IL-4- and IL-13-responsive cells. *J Immunol*. 2003;171(5):2684–2693.
 51. Gharae-Kermani M, Nozaki Y, Hatano K, Phan SH. Lung interleukin-4 gene expression in a murine model of bleomycin-induced pulmonary fibrosis. *Cytokine*. 2001;15(3):138–147.
 52. Huaux F, Liu T, McGarry B, Ullenbruch M, Phan SH. Dual roles of IL-4 in lung injury and fibrosis. *J Immunol*. 2003;170(4):2083–2092.
 53. Singh B, Kasam RK, Sontake V, Wynn TA, Madala SK. Repetitive intradermal bleomycin injections evoke T-helper cell 2 cytokine-driven pulmonary fibrosis. *Am J Physiol Lung Cell Mol Physiol*. 2017;313(5):L796–L806.
 54. Fichtner-Feigl S, Strober W, Kawakami K, Puri RK, Kitani A. IL-13 signaling through the IL-13alpha2 receptor is involved in induction of TGF-beta1 production and fibrosis. *Nat Med*. 2006;12(1):99–106.
 55. Loke P, Nair MG, Parkinson J, Guiliano D, Blaxter M, Allen JE. IL-4 dependent alternatively-activated macrophages have a distinctive in vivo gene expression phenotype. *BMC Immunol*. 2002;3:7.
 56. Hashimoto S, Gon Y, Takeshita I, Maruoka S, Horie T. IL-4 and IL-13 induce myofibroblastic phenotype of human lung fibroblasts through c-Jun NH2-terminal kinase-dependent pathway. *J Allergy Clin Immunol*. 2001;107(6):1001–1008.
 57. Gieseck RL, Wilson MS, Wynn TA. Type 2 immunity in tissue repair and fibrosis. *Nat Rev Immunol*. 2018;18(1):62–76.
 58. Sheridan C. Drugmakers cling to dual IL-13/IL-4 blockbuster hopes. *Nat Biotechnol*. 2018;36(1):3–5.
 59. Lech M, Anders HJ. Macrophages and fibrosis: How resident and infiltrating mononuclear phagocytes orchestrate all phases of tissue injury and repair. *Biochim Biophys Acta*. 2013;1832(7):989–997.
 60. Broekelmann TJ, Limper AH, Colby TV, McDonald JA. Transforming growth factor beta 1 is present at sites of extracellular matrix gene expression in human pulmonary fibrosis. *Proc Natl Acad Sci U S A*. 1991;88(15):6642–6646.
 61. Nagaoka I, Trapnell BC, Crystal RG. Upregulation of platelet-derived growth factor-A and -B gene expression in alveolar macrophages of individuals with idiopathic pulmonary fibrosis. *J Clin Invest*. 1990;85(6):2023–2027.
 62. Giannandrea M, Parks WC. Diverse functions of matrix metalloproteinases during fibrosis. *Dis Model Mech*. 2014;7(2):193–203.
 63. Cao Z, et al. Targeting of the pulmonary capillary vascular niche promotes lung alveolar repair and ameliorates fibrosis. *Nat Med*. 2016;22(2):154–162.
 64. Sinha M, et al. Direct conversion of injury-site myeloid cells to fibroblast-like cells of granulation tissue. *Nat Commun*. 2018;9(1):936.
 65. Maurer B, et al. Fra-2 transgenic mice as a novel model of pulmonary hypertension associated with systemic sclerosis. *Ann Rheum Dis*. 2012;71(8):1382–1387.
 66. Ji WJ, et al. Temporal and spatial characterization of mononuclear phagocytes in circulating, lung alveolar and interstitial compartments in a mouse model of bleomycin-induced pulmonary injury. *J Immunol Methods*. 2014;403(1–2):7–16.
 67. Chakarov S, et al. Two distinct interstitial macrophage populations coexist across tissues in specific subcellular niches. *Science*. 2019;363(6432):eaau0964.
 68. Lucas T, et al. Differential roles of macrophages in diverse phases of skin repair. *J Immunol*. 2010;184(7):3964–3977.
 69. Duffield JS, et al. Selective depletion of macrophages reveals distinct, opposing roles during liver injury and repair. *J Clin Invest*. 2005;115(1):56–65.
 70. Zhu Y, Soderblom C, Krishnan V, Ashbaugh J, Bethea JR, Lee JK. Hematogenous macrophage depletion reduces the fibrotic scar and increases axonal growth after spinal cord injury. *Neurobiol Dis*. 2015;74:114–125.
 71. Gwinn WM, Kapita MC, Wang PM, Cesta MF, Martin WJ. Synthetic liposomes are protective from bleomycin-induced lung toxicity. *Am J Physiol Lung Cell Mol Physiol*. 2011;301(2):L207–L217.
 72. Borthwick LA, et al. Macrophages are critical to the maintenance of IL-13-dependent lung inflammation and fibrosis. *Mucosal Immunol*. 2016;9(1):38–55.
 73. Wernig G, et al. Unifying mechanism for different fibrotic diseases. *Proc Natl Acad Sci U S A*. 2017;114(18):4757–4762.
 74. van der Velden JL, et al. JNK inhibition reduces lung remodeling and pulmonary fibrotic systemic markers. *Clin Transl Med*. 2016;5(1):36.
 75. Specks U, Nerlich A, Colby TV, Wiest I, Timpl R. Increased expression of type VI collagen in lung fibrosis. *Am J Respir Crit Care Med*. 1995;151(6):1956–1964.
 76. Xu X, et al. Evidence for type II cells as cells of origin of K-Ras-induced distal lung adenocarcinoma. *Proc Natl Acad Sci U S A*. 2012;109(13):4910–4915.